CHAPTER TWENTY ONE

5f-ELECTRON PHENOMENA IN THE METALLIC STATE

A. J. Arko, John J. Joyce, and Ladia Havela

21.1 INTRODUCTION

In this chapter, the properties of actinides in the metallic state will be reviewed with an emphasis on those properties which are unique or predominantly found in the metallic solid state. Such properties include magnetism, superconductivity, enhanced mass, spin and charge-density waves, as well as quantum critical points. An introduction to fundamental condensed matter principles is included to focus the discussion on the properties in the metallic state. Systematics of the actinide 5f electronic structure will be presented for elements, alloys, metallic, and semi-metallic compounds so as to elucidate the unique characteristics that arise from the properties of actinides and 5f electrons in a periodic potential.

There are two defining characteristics to materials in the metallic state: first, the material exhibits a periodic potential which controls much of the electronic structure, and second, there is a finite density of electronic states at the chemical potential which influences, among other properties, the thermodynamic and

transport characteristics. For the early actinide metals, these two characteristics are often manifested as narrow bands containing a substantial 5f electron component. Complexity in material properties often arises when competing or overlapping energy scales are available. In the metallic state, with a continuum of electron energy levels available, there is the possibility for interaction of charge with spin and lattice degrees of freedom. Because the actinides have an open 5f electron shell which, in the metallic state, often straddles the boundary between localized and itinerant character, the interplay between spin, charge, and lattice degrees of freedom leads to varied and interesting properties. In order to better understand the controlling role of the 5f electrons in the metallic state, one should look beyond the elements and beyond standard temperature and pressure. To elucidate the fundamental properties of 5f electrons in the metallic state, we consider the actinide elements at low temperature and high pressure. An additional dimension to the understanding of the 5f metals can be attained by considering the actinide elements in a metallic host matrix, e.g. alloys and compounds.

Atoms in a closely spaced periodic environment (crystalline condensed matter) experience an overlapping of outer electron shells with neighboring atoms. If the outer shells are open, then these electrons are shared between neighboring atoms and can travel from atom to atom through the periodic array. This sharing of electrons, a form of bonding, becomes the glue that holds the atoms together. In the crudest sense, this is the metallic state. Here attention is given to those atoms (materials) whose outer shell comprises an unfilled 5f shell, namely, actinide materials. A thorough treatment of the subject covers volumes (Kittel, 1963, 1971; Ziman, 1972; Ashcroft and Mermin, 1976; Harrison, 1980, 1999), so the overview presented here is cursory. The intent is primarily to cover those aspects of the metallic state that differentiate 5f electron systems from simpler metals containing only s, p, or d electrons, since many properties of 5f systems appear anomalous by comparison.

In the atomic and molecular configurations of f-electron materials, the highly directional nature of the f-orbitals plays a central role in the unique properties of the lanthanides and actinides. In the metallic state, however, it is widely accepted that it is the very limited radial extent of the 5f wave functions relative to the s, p, or d wave functions of the valence band that is at the heart of the exotic phenomena (consequently the 5f electrons are nearly localized), though the understanding of the actinides and their compounds is still incomplete. These metals and their compounds are among the most complex in the periodic table, displaying some of the most unusual behaviors relative to non-f systems, such as very low melting temperatures, large anisotropic thermal expansion coefficients, very low-symmetry crystal structures, many solid-to-solid phase transitions, exotic magnetic states, incommensurate charge-density waves, etc. Some insights can be gained by using the 4f series as a guide, but the comparison is limited since the radial extent of the 4f electrons is even smaller than that of the 5f electrons.

A comprehensive picture of actinides in the metallic state is slowly emerging. Many of the very unusual properties appear to be a direct consequence of the formation of extremely narrow 5f bands in which the electrons are not completely free. Rather, their motion is affected by the presence of neighboring 5f electrons. This differs from the lanthanide metals whose 4f electrons tend to be localized in atomic states except perhaps for Ce and Yb (Gschneidner and Eyring, 1993).

In recent years, there have been many advances in the theoretical capability to calculate the electronic structure of materials that form narrow bands. In particular, extensions to density functional theory (DFT) now allow the inclusion of some of the electron–electron interactions that previously were the exclusive domain of many-body physics. Yet even this approach often proves insufficient.

The problem of narrow bands or localization of electrons in an unfilled shell is strongly related to magnetic properties as well. However, there is a fundamental difference between band magnetism and localized magnetism. Although the electronic and magnetic properties of a material are related, the pervasiveness and sheer volume of unusual magnetic behavior observed in the 5f series suggest that they be treated separately.

21.2. OVERVIEW OF ACTINIDE METALS

The anomalous nature of the electronic properties of the 5f series of metals is apparent when considering the electrical resistivity, atomic volume (or equivalently the Wigner–Seitz radius), and a composite crystallographic phase diagram of the actinide metals through Cm. These physical properties are shown in Figs. 21.1–21.3. While these data have been presented on numerous occasions, they remain most illuminating, clearly showing a transition from itinerant (participating in bonding) behavior of the 5f electrons in the light actinides to localized (limited to an atomic site) behavior beyond Pu. It is the transition region that is least understood and where much of the anomalous behavior is centered.

Fig. 21.1 shows the electrical resistivity, ρ, as a function of temperature for the actinides through Cm (the last element obtained in sufficient bulk to allow such measurements). One immediately sees that the overall resistivity increases dramatically up to α-Pu (the low-temperature stable phase of Pu) and then begins to drop for Am. The α-Pu value of 150 $\mu\Omega$ cm ($\mu\Omega$ cm) is much higher than that of Cu (as a material with conventional metallic properties) where the room temperature value is of the order of 1 $\mu\Omega$ cm. The resistivity is intimately tied to the electronic structure of the material and several models ranging in complexity detail the relationship between resistivity and electronic structure. Within the free-electron model, ρ is related to the relaxation time τ of electrons

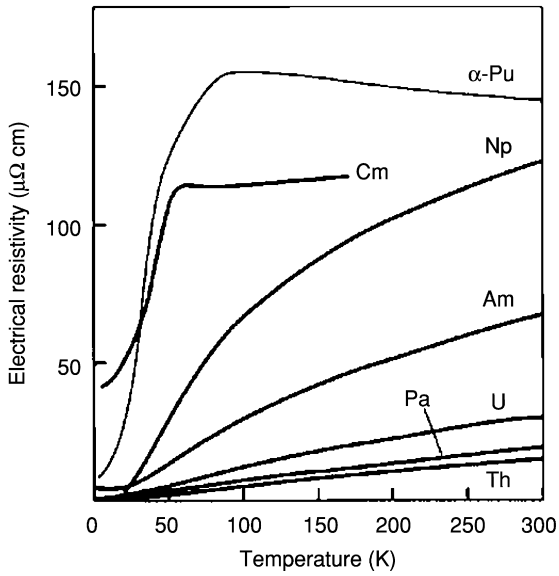

Fig. 21.1 *Electrical resistivity as a function of temperature between* 0 *and* 300 K *for the actinides metals Th through Cm* (*after Hecker,* 2001).

and mean free path defined as $\lambda = v_F\tau$, where v_F is the velocity of electrons at the Fermi surface, called Fermi velocity, by the relationship

$$\rho = m^*/Ne^2\tau \tag{21.1}$$

where m^* is the effective mass of electrons of charge e whose density is N. Clearly the mean free path of conduction electrons in 5f metals is very short and τ is the time between two scattering events compared to normal metals. It is shortest for α-Pu and begins to increase again with Am. Indeed, for α-Pu the mean free path of the conduction electrons is no more than the interatomic spacing. One can hardly call these free electrons.

Additionally, the α-Pu resistivity increases with decreasing temperature, an effect contrary to normal metals like Cu, while it appears relatively normal for Th through U. Such a negative temperature dependence is often associated with magnetic scattering of electrons (thus decreasing their mean free path) although experimental evidence indicates a lack of magnetism in Pu metal.

The Wigner–Seitz radius (Wigner and Seitz, 1933), or the equilibrium atomic volume of an atom in a metallic lattice, is likewise instructive, especially when compared to the volumes occupied by atoms in metals with an open 5d or 4f shell. Fig. 21.2 compares the Wigner–Seitz radius of the lanthanides and actinides with those of the 5d transition metals. It was shown by Friedel (1969) that the atomic volume should display a parabolic dependence with increasing atomic number Z as one fills an open shell of electrons involved in bonding

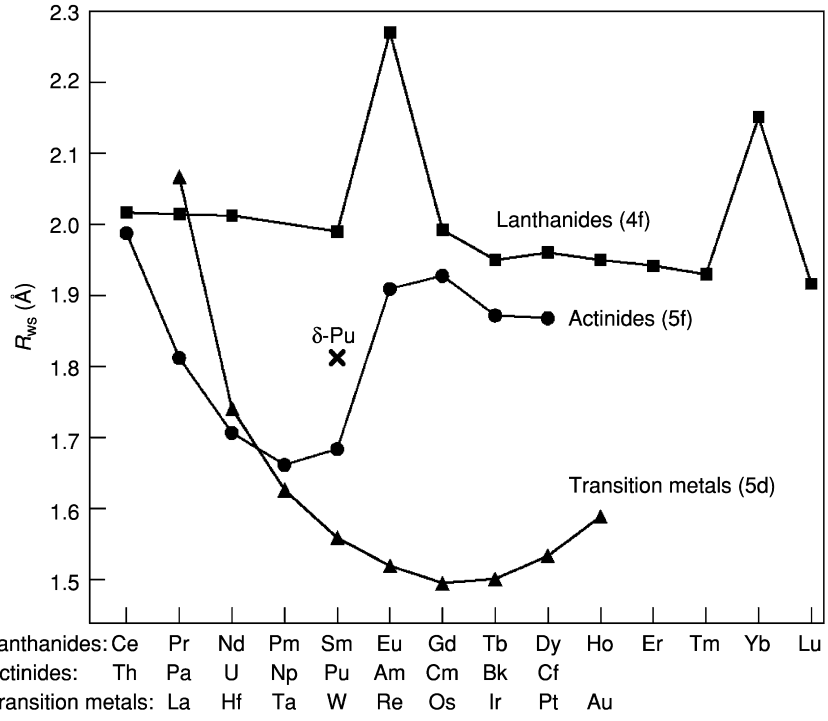

Fig. 21.2 *The Wigner–Seitz radius* (R_{WS}) *for the lanthanides, actinides and the* 5*d transition metal series. The transition metals show a parabolic dependence with bonding d-orbitals in accordance with the predictions of Friedel. The lanthanides display a nominally constant volume with non-bonding 4f states. The actinides show mixed character with Th through* α*-Pu on the bonding Friedel curve while Am–Cf look lanthanide-like with a non-bonding f-character* (*courtesy of Los Alamos Science*).

and conduction (i.e. the 5d electrons in Fig. 21.2). This is attributed to an increasing nuclear charge with its increasing Coulomb attraction, which is not completely screened by outer electrons shared by their neighbors, thus resulting in a volume contraction. But then, as the shell fills, the screening is again effective and the atom relaxes.

If, on the other hand, the outer electrons are instead localized as is the case of the 4f electrons in lanthanides, then the nuclear charge for each value of Z is effectively screened by the localized electrons, and the atomic volume remains unaffected as Z increases. This is clearly evident for the lanthanides in Fig. 21.2, except for Eu and Yb, exhibiting valency irregularities (the metals are divalent, not trivalent as the other lanthanides). The atomic volumes of early actinides appear to follow a parabolic curve up to the metal Np, suggesting 5f participation in bonding, but then begin to strongly deviate, behaving more like the

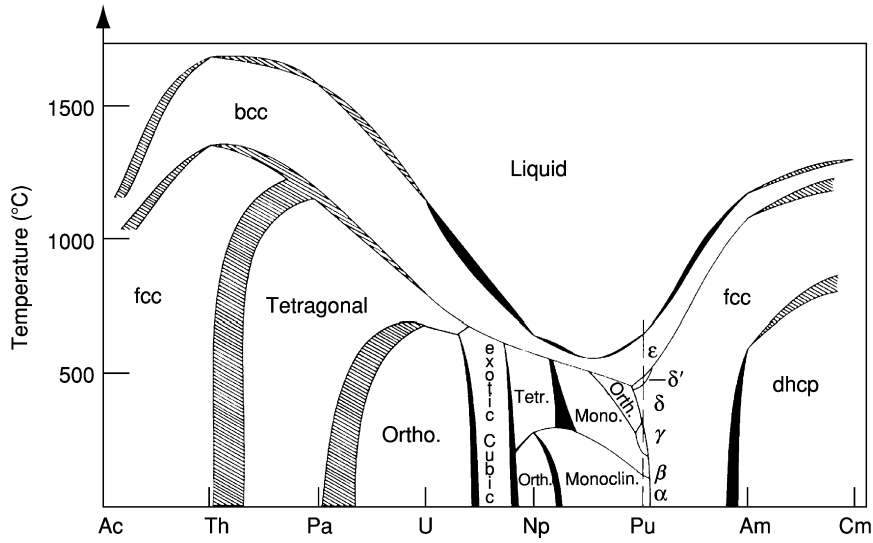

Fig. 21.3 *The binary phase diagram for the actinides Am through Cm showing the reduction in melting point and increase in complexity of the crystal structure and phases as the series moves from bonding* (*Ac–U*) *through localized* (*Am, Cm*) *with Pu having the lowest symmetry* α*-phase as well as the lowest melting point and six solid state allotropes* (*after Smith and Kmetko,* 1983).

localized 4f electrons beyond Pu (i.e. the atomic volumes remain relatively constant with increasing Z). It is as if there were two distinct 5f series: the first ending with Np and the second beginning with Am. In the intermediate region, the various phases of Pu are found, and also much of the correlated electron behavior of interest in this chapter.

The abrupt ending of the parabolic dependence of the equilibrium volumes of the actinides between plutonium and americium differentiates them from the lanthanides and the transition metals. But in addition, the transition metals and actinides also differ in their low-temperature crystal structures. The transition metals form close-packed, high-symmetry structures, such as hexagonal close-packed (hcp), face-centered cubic (fcc), and body-centered cubic (bcc), whereas the light actinides form at low temperatures low-symmetry, open-packed structures. For instance, protactinium forms a body-centered tetragonal (bct) structure, and uranium and neptunium form orthorhombic structures with two and eight atoms per cell, respectively. These data suggest that anomalous behavior already starts in the light actinides where many compounds of the light actinides display strongly correlated electron behavior (Ott and Fisk, 1987; Stewart, 2001).

The crystal structures, along with alloying information, are summed up in the composite phase diagram of Fig. 21.3 (Smith and Kmetko, 1983).

This phase diagram is composed of a series of binary phase diagrams of adjacent actinide metals from Ac to Cm plotted side by side (the x-axis between any two adjacent metals varies from 0 to 100% of the content of the heavier metal). The shaded areas having no crystal structure label represent areas of uncertainty.

In the early part of the series (between Ac and Th) structures are obtained somewhat similar to transition metals while beyond Am, typical structures of the rare earth metals are found. Indeed, it appears that beyond Am the anticipated 'second rare earth series' is obtained. In the region of Np and Pu, however, striking deviations from normal behavior are observed. The most obvious is the large drop in the melting temperature, reaching a value as low as 600°C near Np and Pu. Equally anomalous in this region, however, are the large number of allotropes, or solid-state crystalline phases. In fact, the actinides have the largest number of allotropes of any series in the periodic table. Also in this region one obtains the highest number of bonding f-electrons.

Many of these relevant parameters to actinide metals are captured in Table 21.1. Note the appearance of magnetism in the second rare earth series above Am, as well as the absence of many-body ordering phenomena in Pu and Np and the superconductivity in the light actinides (Am would nominally be magnetic if not for a fortuitous $J = 0$ ground state allowing for superconductivity). The occurrence of interesting electronic properties increases enormously as one changes from the pure actinide elements to actinide alloys and compounds.

Figs. 21.1–21.3 are entirely consistent with each other. The metallic radii are smallest at the crossover to localization, and as shown in Fig. 21.2, the low-temperature phases of the heavier actinides (beginning with americium) form dhcp structures. As in most metals, it is the bcc phase that forms prior to melting. However, the temperature range over which this phase is formed in the actinides is very small compared to transition metals and appears to be another signature of narrow bands, as described below (Wills and Eriksson, 2000).

A detailed description of the properties for Pu metal is presented in Chapter 7. Here the emphasis is on overall 5f electronic properties and their differences from simpler metals. To recognize these differences, a short discussion of free electron and condensed-matter behavior is presented. The papers by Boring and Smith (2000), and Wills and Eriksson (2000) serve as more detailed references and the main sources for this material.

21.3 BASIC PROPERTIES OF METALS (FREE-ELECTRON MODEL)

21.3.1 Formation of energy bands in simple metals

In general, most materials (metal or non-metal), when condensed in the solid state, form a crystalline array of repeating unit cells. Indeed, it is this repetition in space that allows for the mathematical determination of the electron wave

Table 21.1 *Properties of actinide metals.*

Element	*Melting point*[a,b] (K)	*Enthalpy of sublimation*[a,b] *at* 298.15 K (kJ mol^{-1})	*Lattice symmetry*[a–c]	*Temperature range* (K)[a–c]	*Lattice constants*[a,c] a_o (Å)	b_o (Å)	c_o (Å)	β (deg)	*X-ray density* (g cm^{-3}) (calc)	*Z (atoms per unit cell)*[a,c]	*Metallic radius CN* 12 (Å)[a,c,e]	*Bulk modulus* (GPa)[f]	*Low T specific heat coeff.* γ (mJ/mol K^2)[g]	χ_0 (10^{-4}emu/mol)[h,i]	μ_{eff} (μ_B)[j]	*Ordering temp.* (K)[l]
actinium	1323 ± 50	418 ± 20	fcc		5.315(5)				10.01	4	1.878					
thorium		602 ± 6	α, fcc	below 1633	5.0842				11.724	4	1.798	59.0(9)	4	.93		1.37 SC
	2023 ± 10		β, bcc	1633–2023	4.11 (1450K)					2	1.80					
protactinium		570 ± 10	α, bc tetrag.	below 1443	3.929		3.241		15.37	2	1.643	118(2)	6.6	2.7		1.4 SC
	1845 ± 20		β, bcc or fcc	1443–1845												
uranium		533 ± 8	α, orthorh.	below 941	2.854	5.87	4.955		19.04	4	1.542	104(2)	10	3.8		0.68 SC
			β, tetrag.	941–1049	5.656(5) (995K)	10.759(5)	10.759(5)		18.11	30	1.548					
	1408 ± 2		γ, bcc	1049–1408	3.524(2) (1078K)				18.06	2	1.548					
neptunium		465.1 ± 3.0	α, orthorh.	below 553	6.663 (293K)	4.723	4.887		20.48	8	1.503	118	14	5.5		
			β, tetrag.	553–849	4.897 (586K)		3.388		19.38	4	1.511					
	912 ± 3		γ, bcc	849–912	3.518 (873K)				18.08	2	1.53					
plutonium		349.0 ± 3.0	α, monocl.	below 397.6	6.183 (294 K)	4.822	10.963	101.79	19.85	16	1.523	43(2)	17(1)	5.3		
			β, monocl.	397.6–487.9	9.284 (463K)	10.463	7.859	93.13	17.71	34	1.571			5.5		

			γ, orthorh.	487.9–593.1	3.159 (508K)	5.768	10.162	17.15	8	1.588			5.2		
			δ, fcc	593.1–736.0	4.637 (593K)			15.92	4	1.640	29.9	64(3)	5.1		
			δ′, bc tetrag.	736.0–755.7	3.34 (738K)		4.44	16.03	2	1.640			5.1		
	913 ± 2		ε, bcc	755.7–913.0	3.6361 (763K)			16.51	2	1.592			5.2		
americium		283.8 ± 1.5	α, dhcp	below 1042	3.47		11.25	13.67	4	1.730	30	2	6.8		0.79 SC
			β, fcc	1042–1350	4.89			13.69	4	1.730					
	1449 ± 5		γ, bcc?	1350–1449	unknown										
curium		384 ± 10	α, dhcp	below 1568	3.500(3)[d]		11.34(1)[d]	13.5	4	1.743	33			8.07[k]	52 AF[k]
	1619 ± 50		β, fcc	1568–1619	5.065			12.7	4	1.782					
berkelium		310 ± 10	α, dhcp	below 1250	3.416(3)		11.069(7)	14.79	4	1.704	25			8.5	34 AF
	1323 ± 50		β, fcc	1250–1323	4.997(4)			13.24	4	1.767					
californium		196 ± 10	α, dhcp	below ~973	3.384(3)		11.040	15.1	4	1.691	50			9.7	51 FM
	1173 ± 30		β, fcc	~973–1173	4.78(1)			15.1	4	1.69					
einsteinium	1133	130 ± 10	fcc		5.75(1)			8.84	4	2.03				11.3?	

[a] Values from Chapters 2–12.
[b] Values taken from Chapter 19.
[c] Values taken from Chapter 22, at 298.15 K, except as noted.
[d] From Stevenson and Peterson (1979).
[e] See also Zachariasen (1973).
[f] Th (Benedict and Holzapfel, 1993); Pa, U, and Am (Lindbaum *et al.*, 2003); Np (Dabos *et al.*, 1987); α-Pu (Dabos-Seignon *et al.*, 1993); δ-Pu, from measurements on a single crystal of Pu with 3.3 atomic% Al (Ledbetter and Moment, 1976); Cm, Bk, and Cf (Benedict, 1987).
[g] Th (Gordon *et al.*, 1966); Pa (Spirlet *et al.*, 1987); U (Bader *et al.*, 1975); Np (Mortimer, 1979); α-Pu and δ-$Pu_{0.95}5Al_{0.05}$ (Lashley *et al.*, 2003); Am (Smith *et al.*, 1979).
[h] Temperature-independent susceptibility χ_0.
[i] Most of these elements show a slight temperature dependence, possibly due to impurities. Data taken from Nellis and Brodsky (1974) except Th (Greiner and Smith, 1971); Pu (Olsen *et al.*, 1992).
[j] Effective magnetic moment in units of Bohr magnetons (μ_B). Different samples show rather different values. Representative values given. Data taken from Chapter 20 except as noted.
[k] This Cm value is from Kanellakopulos *et al.* (1975).
[l] Superconducting (SC), antiferromagnetic (AF), ferromagnetic(FM). Data for ordering temperatures of the transamericium actinides are from Chapter 20 except as noted.

functions to within a phase factor. These cyclic wave functions are called Bloch states after Felix Bloch, who first introduced them (Bloch, 1928). The simplest elements, with a single outer electron, such as lithium or sodium, typically form cubic crystal structures at room temperature. The outer electrons from their atomic valence shells become conduction electrons traveling almost freely through the lattice. That is, these valence electrons occupy one-electron Bloch states, and they are therefore responsible for bonding in the solid.

A logical progression can be followed for band formation starting from the isolated atom, to molecules and finally, band formation and the formation of Bloch states in a metal. In the isolated atom, the electrons exist in a potential well with well-defined energy levels or states. The levels representing the outermost, or valence states, are responsible for bonding. Considering first the case of only two isolated atoms (i.e. molecular case), when two atoms are brought together, their outer electron wave functions (orbitals) overlap, and the valence electrons feel a strong electrostatic pull from both nuclei (typically depicted as a double-well electrostatic potential). The atomic orbitals combine to form molecular orbitals that may bind the two atoms into a diatomic molecule. The single atomic energy level splits into two allowed states: one lower in energy, or bonding, and the other higher in energy, or antibonding. The energy difference between these two levels is proportional to the amount of overlap of the two-electron atomic orbitals, and the molecular orbitals (wave functions) corresponding to the bonding and antibonding energy levels are the sum and difference, respectively, of the atomic orbitals.

If one generalizes to the case of N atoms brought close together to form a perfect crystal, the single valence electron now sees the periodic electrostatic potential due to all N atoms (where N is a number of order 10^{23}). The wave function (Bloch state) is now a combination of overlapping wave functions from all the atoms and extends over the entire volume occupied by those atoms. As in the molecular case, that wave function can be a bonding state or an antibonding state. The original atomic valence levels generalize to a band of very closely spaced energy levels, half of them bonding and half of them antibonding, and the width of the energy band is approximately equal to the energy splitting between the bonding and antibonding energy levels in the diatomic molecule. This broad band forms whether the crystal is an insulator, a metal, or a semiconductor, the metal being the case where the uppermost band is not completely occupied by the available electrons.

Because in a macroscopic sample the number of energy levels in the energy band is large (approximately 10^{23}, corresponding to the number of valence electrons in the crystal) and the spacing between these energy levels is small, the electron energies may be considered to be a continuous variable. The number of electron energy levels per unit energy is then described in terms of a density of states (DOS) that varies with energy. Because each electron must have a slightly different energy (the Pauli exclusion principle), electrons fill up

the energy levels one by one, in the order of increasing energy (in accordance with the Fermi–Dirac statistics). This concept will be detailed below.

21.3.2 Brillouin zones

A Bloch state, or the three-dimensional extended wave function of a valence electron in a solid, may be represented in one dimension by the valence electron wave function appearing at every atomic site along a line of atoms, but its amplitude is modulated by the plane wave $e^{i\boldsymbol{k}\cdot\boldsymbol{r}}$ where $\boldsymbol{k}$ is the momentum of the allowed state and $\boldsymbol{r}$ is the position vector. As mentioned before, this general form for a Bloch state in a solid emerges from the requirement of translational invariance. That is, the electron wave function in a given unit cell must obey the Bloch condition

$$u_k(r + \boldsymbol{T}_n) = u_k(r), \tag{21.2}$$

where $\boldsymbol{T}_n$ is a set of vectors connecting equivalent points of the repeating unit cells of the solid and u_k is the one-electron potential. The wave function must therefore be of the form

$$\Psi_k(r) = e^{i\boldsymbol{k}\cdot\boldsymbol{r}} u_k(r), \tag{21.3}$$

where a plane wave with wave vector $\boldsymbol{k}$ modulates the atomic wave function in a solid. The wave vector $\boldsymbol{k}$, or the corresponding crystal momentum $\boldsymbol{p} = h\boldsymbol{k}$, is the quantum number characterizing that Bloch state, and the allowed magnitudes and directions of $\boldsymbol{k}$ reflect the periodic structure of the lattice. Indeed, the momentum vectors $\boldsymbol{k}$ are related to the vectors of the unit cell in an inverse fashion. For example, if $\boldsymbol{T}_n$ is the vector in a unit cell in real space (e.g. along the [100] direction) which connects equivalent points, then the corresponding crystal momentum vector is $2\pi/\boldsymbol{T}_n$ which connects equivalent points in momentum space (i.e. a reciprocal lattice vector). The most basic periodic crystal unit is not necessarily the unit cell. Often a unit cell can be further reduced to a primitive cell, or a Bravais lattice, which defines the most basic repetitive unit. One can then derive a set of real space vectors that define a Bravais lattice. The inverse of these vectors defines the most basic repetitive unit in momentum space – the Brillouin zone. Energy bands are defined within this three-dimensional reciprocal, or momentum space having axes of k_x, k_y, and k_z. For a simple cubic unit cell, both the primitive cell in real space and its associated Brillouin zone are likewise simple cubic. Allowed energy band states, of course, can have a continuously varying set of momentum states, with the reciprocal lattice vectors being only a special set of crystal momenta defining the Brillouin zone boundaries along various high-symmetry directions. Within a solid, the periodic, crystalline symmetries replace the more common localized potentials of atoms and molecules. Also, the crystal momentum quantum numbers replace the usual orbital angular-momentum components. Within this framework, the metallic,

condensed matter properties of magnetism, superconductivity, enhanced mass, spin, and charge-density waves are quantified.

21.3.3 Complex and hybridized bands

The electronic structure gets more complicated in metals containing more than one type of valence electrons. A typical band structure for uranium metal (Wills and Eriksson, 2000) is shown in Fig. 21.4. Here the multiple overlapping bands are created when the conduction electrons in a solid originate from various s, p, d, and f valence orbitals of an atom. In general, the width of each band increases as the interatomic distance decreases and the overlap of the wave functions increases. Also, the s and p bands are always wider (span a wider energy range) than the d band, which in turn is always wider than the f band, reflecting the larger radial extent of the non-f wave functions. The overlapping bands in Fig. 21.4 portray a case where at a given value of $\boldsymbol{k}$ (a position vector in momentum space) one has wave functions of more than one orbital symmetry (angular momentum) but having nearly the same energy. This implies that the Bloch functions with a given quantum number (wave vector) $\boldsymbol{k}$ could be represented as a linear combinations of states originating from the s, p, d, and f atomic orbitals. In other words, the Bloch states could be 'hybridized' states containing many angular-momentum components, in contrast to atomic

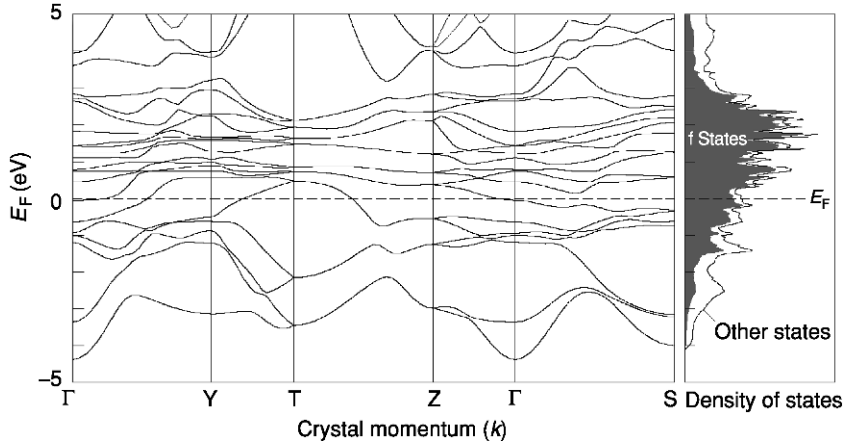

Fig. 21.4 *An electronic structure calculation for α-U metal including energy bands and the density of states. The DFT predictions for the energy bands* E(**k**) *are plotted along several different directions in the unit cell of the reciprocal lattice. The labels on the* **k***-axis denote different high-symmetry points in reciprocal space:* $\Gamma = (000)$, $Y = (100)$, $T = (111)$. *The narrow bands close to the Fermi level are dominated by the* 5*f levels. Some of the bands cross the Fermi level making α-uranium a metal. The shaded area for the density of states curve represents the* 5*f orbital contribution* (*courtesy of Los Alamos Science*).

orbitals that contain only one angular-momentum component. The angular-momentum mixture for a given band can vary from point to point in momentum space. Near $\boldsymbol{k}$-values where several bands are nearly degenerate one obtains a strong admixture, while for regions in $\boldsymbol{k}$-space where bands do not cross each other, the orbital symmetry of a band may contain only a single component. The dashed line in Fig. 21.4 is the Fermi energy (E_F) and separates the occupied from unoccupied energy levels.

The 5f states dominate the bonding primarily because there are three 5f electrons per atom and only one d-electron per atom occupying the Bloch states and participating in bonding. The narrow 5f band is referred to as the dominant band. Because narrow bands correspond to small overlaps of wave functions, these 5f band electrons may be easily pushed toward localization by various effects, in which case they do not contribute to bonding. Compared with the band widths of non-f metals, the actinide 5f bands are narrow and reflect the limited wave function overlap between f-orbitals on adjacent sites. The narrowness of the 5f bands and the proximity to the Fermi energy make the 5f bands central to understanding the actinide metallic state.

21.3.4 Density of states

A very useful concept to consider is the concept of the density of allowed energy states per unit energy interval. Recall that the allowed states in a band are not actually continuous, but are very closely spaced. Since each band of allowed states may contain two electrons from each atom (spin up and spin down), one can see that bands that disperse rapidly with energy will have fewer allowed states per unit energy interval than slowly dispersing or 'flat' bands. The right frame of Fig. 21.4 shows the DOSs resulting from the multiband structure on the left panel of Fig. 21.4. Note that the 5f states outnumber all the others at the Fermi energy E_F (see below for description). If an energy sub-band is filled (two electrons of opposite spin occupy all its energy levels), there will be no electron density at E_F and the solid is an insulator. If a band is only partially filled, the solid is a metal.

21.3.5 The Fermi energy and effective mass

Electrons, being spin-½ particles, obey Fermi statistics with the occupation of states occurring in order of increasing energy. The mathematical expression for Fermi–Dirac statistics is

$$f = 1/[\exp\{(E - E_F)/k_B T\} + 1]. \tag{21.4}$$

where k_B is the Boltzmann factor. The probability, f, for occupation of states at $T = 0$ is unity up to the Fermi energy, E_F, and zero above this energy. E_F is defined as the highest occupied energy state in a metal after all the electrons in a crystal (or in a box in the case of true free electrons) have been accounted for at

$T = 0$. As the atomic levels are filled up and the band states (i.e. the valence states involved in bonding) become occupied, the energy or momentum of a band electron from a particular atom is not precisely known. One only knows that it occupies one of the near continuum of allowed energies in a band and that the lowest states in a band must be occupied first.

In many elements (e.g. the alkali metals), the atom has only one electron to contribute to the uppermost or valence band. In that case, the uppermost band is unfilled (half filled for the alkali metals). More importantly, in the case of complex systems as shown in Fig. 21.4, the complexities introduced by the crystal structure and the subsequent hybridization result in an overlapping of valence bands, such that some states from a higher band actually lie below a lower one. This is clearly shown in Fig. 21.4 where the s–d bands cross the f-bands. In this case, the upper band begins to be filled before the lower one is fully occupied, so that, when all the electrons are exhausted, neither band is filled, and empty states exist just above E_F. The highest occupied energy (at $T = 0$ K) is E_F and the material is a metal because the electrons occupying the highest energy state have many empty allowed states in their vicinity into which they can scatter in order to travel throughout the crystal. By contrast, in the case of insulators where the uppermost band is fully occupied and there is an energy gap before the next band that is unoccupied, the Pauli exclusion principle prevents the occupation of states that already contain two electrons. Thus the electrons are not free to change states and move throughout the crystal unless they obtain sufficient energy to access an empty state beyond the energy gap between filled and empty states.

At finite temperature T, some electrons within k_BT below E_F can occupy empty states within k_BT above E_F. This is shown in Fig. 21.5 where the Fermi–Dirac distribution function has been convoluted with a model DOS. The probability of occupation of states below E_F is unity except within a few k_BT of E_F where some electrons can scatter into empty states within a few k_BT above E_F. Fig. 21.5 shows that electrons with binding energies higher than $(E_F - k_BT)$ contribute to the bonding, and only the narrow stripe just above E_F is responsible for the metallic behavior. Most of the properties of a metal (excluding magnetism) are determined by the band states within a few k_BT of E_F. The sudden drop in occupation is referred to as the Fermi edge. One immediately begins to see that densities of states whose width is of the order of k_BT will be dramatically affected by temperature. Of course, in complex systems electrons from more than one band and angular momentum are allowed to scatter into empty states. The substantive effects of the Fermi function are generally considered to occur within $\pm 2.2k_BT$ of the Fermi level. These values represent the 90% (below E_F) and 10% (above E_F) occupancy values for electron states at a finite temperature T.

Within the free-electron model (i.e. free-electron gas in a box) the energy is measured from the bottom of the free-electron band parabola. The electron energy dispersion is

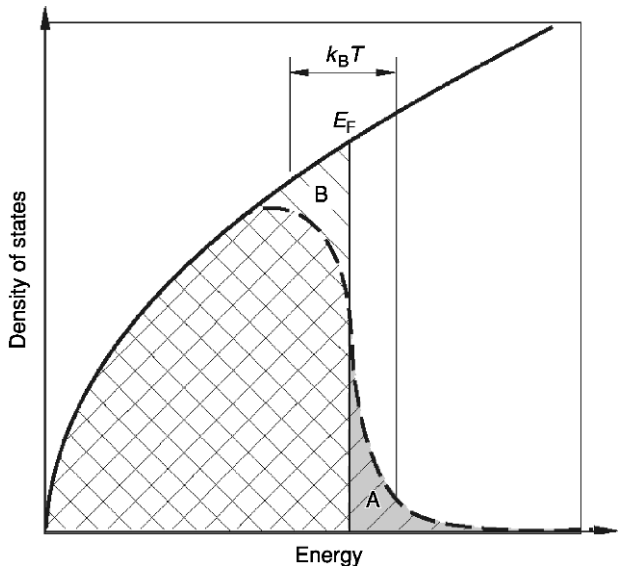

Fig. 21.5 *The solid line is the density of states for a free-electron gas plotted as a function of one-electron energy. At* T = 0, *electrons occupy all the states up to the Fermi energy* E_F. *The dashed curve shows the density of filled states at a finite temperature* T. *Only electrons within* k_BT *of the Fermi level can be thermally excited from states below the Fermi energy* (*region B*) *to states above that level* (*region A*) (*courtesy of Los Alamos Science*).

$$E = (\boldsymbol{p})^2/2m^*, \tag{21.5}$$

where $\boldsymbol{p}$ is the momentum and m^* is effective mass of the electron. The uppermost filled level is at the Fermi energy and is given by $E_F = (\boldsymbol{p}_F)^2/2m^*$, where $\boldsymbol{p}_F$ is the momentum of this uppermost level. Here E_F essentially corresponds to the bandwidth of the occupied states. If one then takes a repetitive box (i.e. a crystal lattice) one fulfills the requirement of periodicity, so that a free-electron parabola exists in each box – or Brillouin zone. The parabola from each Brillouin zone may extend through many other adjacent zones so that the resulting band (reduced or folded back into the first zone by virtue of periodicity) can be very complex. Nonetheless, in the case of alkali metals and other simple metals the bandwidth definition of the Fermi energy is still often used. The crystal momentum is zero at the center of the reciprocal lattice where $k = 0$. In a complex band system such as shown in Fig. 21.4, this definition loses some of its meaning. Nonetheless, if one adheres to this definition, one may define the Fermi temperature, $T_F = E_F/k_B$, as well as the Fermi velocity, $v_F = [2E_F/m^*]^{1/2}$. The use of m^* rather than m_o is appropriate in the formula because even the periodic crystal potential has some effect on the effective mass. Indeed many of

the properties of the free-electron model can be transferred to real material systems by substituting m^* for m_o.

The effective mass is essentially a measure of the interactions (correlations) that slow down (sometimes even speed up) the electron motion. Because of electron–electron interactions $\boldsymbol{v}_F$ can be smaller for a given $\boldsymbol{p}$, sometimes much smaller, than predicted by free-electron theory. It is as if the electron were much heavier than a free electron. Formally,

$$m^* = \hbar/(d^2E(k)/dk^2), \tag{21.6}$$

where $E(k)$ is a band that crosses the Fermi level and the derivative is evaluated at the Fermi level. It is easy to see that a very slowly dispersing or nearly flat band (this is obviously no longer a free-electron parabola) will have a much larger m^* than a rapidly varying band such as is found for s- and p-electrons where the wave function overlap is large. Correlations can be viewed as effectively resulting in a flattening of the bands at the Fermi edge.

21.3.6 Fermi surface

If one draws the energy band states in three dimensions defined by the crystal momentum $\hbar\boldsymbol{k}$ (in Fig. 21.4 they are shown in one dimension along a major symmetry axis) and connects all the points where each band crosses E_F, then these points trace out a surface in momentum space (or $\boldsymbol{k}$-space) known as the Fermi surface. In the free-electron model, each state on the Fermi surface corresponds to an electron having a constant absolute value of Fermi momentum $|\boldsymbol{p}_F|$ with kinetic energy given by the free particle formula above. In the case of a free-electron parabolic band, the Fermi surface is essentially a sphere, provided that the Fermi momentum $\boldsymbol{p}_F$ exists within the first Brillouin zone. If it extends into the next zone, one may still simply reconstruct the Fermi surface from a lattice of overlapping spheres. Again, in complex systems where several bands of differing angular momentum and bandwidth cross the Fermi energy, the topology of the Fermi surface can become extremely complex, one cannot use the simple bandwith definition of the Fermi energy, and $\boldsymbol{p}_F$ must be defined for each band.

The topology of the Fermi surface can be experimentally determined by means of de Haas–van Alphen (dHvA) oscillations. While a complete description of this effect is far beyond the scope of this chapter, qualitatively this is a measurement of the oscillatory diamagnetic susceptibility. For metal single crystals at low temperatures in the presence of a changing magnetic field, B, the diamagnetic susceptibility is influenced by B because the presence of B imposes an additional quantum condition on the free-electron orbits. The energy states of the electrons in the allowed orbits are called Landau levels, and these change with changing B. Without going into detail, the changing Landau levels (as B is varied) induce oscillations in the susceptibility, the frequency of

which (proportional to $1/B$) is directly related to the cross-sectional area of the Fermi surface in momentum space. By measuring the oscillations for differing directions of B, one can reconstruct the topology of the Fermi surface. Furthermore, by measuring the amplitude of the oscillations as a function of temperature, it is possible to determine the m^* of the orbiting electrons.

21.3.7 Electronic heat capacity

For a gas of free particles heated from absolute zero to a temperature T, classical statistical mechanics would predict that, on the average, the kinetic energy of each particle would increase by an amount $k_B T$. But because of the Pauli exclusion principle, the electrons obey Fermi–Dirac statistics and only those conduction electrons occupying states within $k_B T$ of the Fermi level E_F can be heated (by phonon scattering) because only they can access states not occupied by other electrons (see Fig. 21.5). The number of electrons that participate in properties such as electrical conduction and electronic heat capacity decreases to a fraction T/T_F of the total number of conduction electrons in the metal. At room temperature, T/T_F is about 1/200 in most metals. Thus, replacing the classical Maxwell–Boltzmann statistics with the Fermi–Dirac quantum statistics implied by the exclusion principle has a profound impact on the electronic properties of metals.

The factor T/T_F shows up explicitly in the low-temperature specific heat of a metal. In general, the specific heat is the sum of a lattice-vibration term (proportional to T^3) and an electronic term γT, which is due to the thermal excitation of the electrons. The classical coefficient of the electronic term is $\gamma = Nk_B$ (where N is the number of conduction electrons) but because of the exclusion principle, it becomes

$$\gamma = 2Nk_B T/T_F, \tag{21.7}$$

and only electrons near the Fermi energy can be excited. Thus, in simple metals obeying the free-electron model, γ is inversely proportional to T_F, or equivalently, E_F, and therefore proportional to m^* (see above), or to the density of electronic states at the Fermi level, $N(E_F)$. The prefactor 2 represents two possible spin directions.

A common unit of γ is (mJ mol^{-1} K^{-2}) and the value is about 1 for a typical free-electron metal like Cu. In strongly correlated actinide materials, values as large as 1000 have been observed. Here electrons behave more like strongly interacting particles of a liquid, e.g. more like a Fermi liquid. Because of interactions, m^* increases and shows an increase in the value of γ over that predicted by the free-electron model. Thus, low-temperature specific heat measurements reveal the strength of the electron–electron correlations in a metal and therefore provide a major tool for identifying unusual metals.

21.3.8 Electrical resistivity

For free electrons the resistivity ρ is given by equation (21.1). In a perfect crystal, electrical resistance would be zero near the classical $T = 0$ limit because the non-interacting conduction electrons, acting as waves, would move through the perfect lattice unimpeded. Above $T = 0$, the thermal excitations of lattice vibrations (phonons) affect the lattice periodicity and thus scatter the Bloch waves which depend on periodicity. Near $T = 0$, in the absence of strong electron–electron (e–e) interactions and impurities, $\rho(T)$ increases as T^5, while at higher temperatures $\rho(T) = AT$, where A is a constant. In general, anything that destroys the perfect translational invariance of the crystal lattice will scatter electrons. This is reflected in the mean free path of electrons, λ, the distance traveled by electrons between scattering events (see equation (21.1)). Foreign atoms, lattice vacancies, more complicated defects such as stacking faults, and finally, magnetic moments in an array without the full symmetry of the lattice can scatter electrons since they destroy the periodicity. Many of these imperfections are temperature-independent and lead to a finite limiting resistance as $T = 0$ is approached, called the residual resistance or ρ_0. Hence, this limit is used as a measure of the quality of metal samples, for which the lowest ρ_0 signifies the most perfect sample. It has been shown that correlated electron materials (and actinide metals in particular, see Fig. 21.1) often have anomalously high $\rho(T)$ and ρ_0 despite very small or zero magnetic moments at low temperatures. For systems with a high $N(E_F)$, strong electron–electron scattering gives rise to a term aT^2, where the prefactor a reflects the e–e correlations so that a/γ^2 is approximately constant for various materials.

21.3.9 One-electron band model

It has been shown that even a free-electron model for a periodic system yields a relatively complex band structure. The periodic potential actually introduces gaps at the Brillouin zone boundaries, and, depending on $\boldsymbol{p}_F$ relative to the zone boundaries, the Fermi surface can be very complicated. To obtain the band structure in materials with several valence electrons having more than one type of angular momentum requires substantial calculations. However, the problem of dealing with 10^{23} electrons can be reduced to a one-electron problem by assuming that an electron sees only an averaged potential between the ions and the remaining electrons, and that this periodic electrostatic potential can be modeled in a self-consistent fashion.

Slater first proposed calculating the electronic states, the energy bands in Fig. 21.4, of solids by the same self-consistent method that had been applied so successfully to describe the electronic states of atoms and molecules (Slater, 1937). In this method, one treats electrons as independent particles and calculates the average Coulomb forces on a single electron. The equation for the one-electron states is essentially the time-independent Schrödinger equation,

$$(T + V_{\text{eff}})\psi_{\text{i}}(\boldsymbol{r}) = E_i\psi_i(\boldsymbol{r}) \tag{21.8}$$

where T is a kinetic energy operator (e.g. $-\hbar^2\nabla^2/2m$ in a non-relativistic approximation and ∇ is the derivative with respect to position, V_{eff} is the average effective potential, and E_i are the eigenstates. The other electrons and all the ions in the solid are the source of these Coulomb forces on one electron and give rise to the V_{eff}. This calculation, repeated for all the electrons in the unit cell, leads to a charge distribution

$$n(r) = \Sigma|\psi_i(\boldsymbol{r})|^2 \tag{21.9}$$

from which a new electrostatic potential seen by the electrons can be obtained as a solution of the Poisson equation. Using the new electrostatic potential, one then repeats the calculations for each electron until the charge density (distribution of electrons) and the crystal potential (forces on the electrons) have converged to self-consistent values. Slater's approach led to all the modern electronic band structure calculations commonly labeled one-electron methods. These one-electron band-structure methods are adaptations of the familiar Hartree–Fock methods that work so well for atoms and molecules. They were put on a more rigorous footing through Kohn's development of DFT. Unlike the genuine Hartree–Fock method, the non-local part of electron–electron interaction is treated less formally, but it includes the long-range screening, unimportant for simple molecules but prominent in the electron gas.

Once a metal is formed, its conduction electrons (approximately 10^{23} per cubic centimeter) can act collectively, in a correlated manner, giving rise to what is called quasiparticle behavior (not determined by averaged electrostatic forces) and to collective phenomena such as superconductivity and magnetism. These phenomena are outside the scope of the independent electron model, which cannot accommodate all the electron–electron interactions found in the actinide series. Many-body interactions do not readily lend themselves to reduction to an average potential. Nevertheless, great strides have been made toward including correlations into the one-electron picture. In particular, DFT described below can incorporate the concept of exchange as well as Coulomb correlation. These electron correlations are described in the next section.

21.3.10 Electron–electron correlations

Electrons in a crystal are simultaneously attracted to the ions and repelled from each other via Coulomb repulsion. To minimize the total energy of the system, the electrons must minimize the electron–electron repulsion while maximizing the electron–ion attraction, and the way to minimize the Coulomb repulsion is for them to stay as far from each other as possible. In calculations on the helium atom it was found that: first, the two He electrons are indistinguishable – that is, electron 1 can be in orbital A or B, and so can electron 2; second, the electrons have to obey the Pauli exclusion principle, which means

that the total wave function for the two electrons has to be antisymmetric, and that antisymmetry implies that the Hamiltonian must contain an exchange term. This exchange term determines the probability that two electrons of the same spin can exist near each other. It is what separates the Hartree–Fock calculations of many-electron atoms from the original Hartree calculations of those atoms.

When the exchange term was included in the calculation of an electron gas, it was found that around each electron, there is a 'hole', or depression in the probability of finding another electron close by. Indeed, this probability was found to be one-half the value it would have without the exchange term. This exchange hole demonstrates that the electron motion of the two electrons is correlated with each other, in the sense that electrons with the same spin cannot get close to each other.

In the 1930's, Wigner performed similar calculations for electrons of opposite spins, which led to a 'correlation' hole (very similar to the exchange hole) for the probability of finding an electron of opposite spin near a given electron (Wigner, 1934). The picture of an exchange hole and a correlation hole around each electron is a great visual image of electron correlations in solids. Modern one-electron calculations include these correlations in an average way because these terms can be calculated from the average electron density around a given electron. The cost in energy of putting two electrons on the same site is referred to as the Coulomb correlation energy.

Several theories will be considered in this chapter that include interactions beyond the one-electron method, these approaches are termed correlated-electron theory. Likewise, any solid (metal, insulator, and so on) that exhibits behavior not explained by either the free-electron model or the one-electron band model is considered a correlated-electron system. If the properties of a solid deviate strongly from the predictions of free-electron or band models (e.g. heavy fermions), that solid is called a strongly correlated system. While many actinide metals and compounds fall within this group, still many others can be described as weakly correlated systems that are quite tractable within the one-electron approach.

21.3.11 Density functional theory

This section concludes with a brief description of DFT, a one-electron band structure approach which includes both exchange and correlation, and which has been very successful in describing weakly correlated systems. Two common variants are used: the local density approximation (LDA), which expresses the exchange and correlation potential, $E_{xc}(n(\boldsymbol{r}))$, as a function of local electron density, while the generalized gradient approximation (GGA) includes, in addition to these terms, the gradient of $n(\boldsymbol{r})$ as well. Formally, as in the Slater approach, the starting point for DFT calculations is the time-independent Schrödinger equation (similar to equation (21.8) above).

One would, in principle, calculate the ground-state (lowest-energy configuration) total electronic energy from

$$H\psi(\boldsymbol{r}_1, \boldsymbol{r}_2, \ldots \boldsymbol{r}_n) = E\psi(\boldsymbol{r}_1, \boldsymbol{r}_2, \ldots \boldsymbol{r}_n)\,, \tag{21.10}$$

where H is the Hamiltonian containing the kinetic energy and all the interactions of the system (i.e. electron–electron correlation and exchange and electron–nuclei interactions) and $\boldsymbol{r}_1,\boldsymbol{r}_2,\ldots \boldsymbol{r}_n$ are the n position vectors. However, in the most generalized form $\psi(\boldsymbol{r}_1,\boldsymbol{r}_2,\ldots \boldsymbol{r}_n)$ is now a many-electron wave function of the n-electron system, and E is the total electron energy of the entire system in the ground state. The input parameters in equation (21.10) are the atomic numbers of the atoms and the geometry of the crystal (the lattice constant, the crystal structure, and the atomic positions). From the solution of this equation, one should, in principle, be able to calculate the equilibrium crystal structure, the cohesive energy, as well as the band structure. Unfortunately, there is no practical way to solve equation (21.10) for a solid.

To get around this problem, Hohenberg and Kohn (1964), Kohn and Sham (1965), and Dreitzler and Gross (1990) pointed out that the total energy of a solid (or atom) may be expressed uniquely as a functional of the electron density (equation (21.9) (i.e. $E = E[n(\boldsymbol{r})]$ just as E_{xc} above). This function can be minimized in order to determine the ground-state energy. Therefore, instead of working with a many-electron wave function, $\psi(\boldsymbol{r}_1,\boldsymbol{r}_2,\ldots \boldsymbol{r}_n)$, one can express the ground-state energy in terms of the electron density at a single point (as in equation (21.9)), where that density is due to all the electrons in the solid.

In addition, Hohenberg and Kohn (1964), Kohn and Sham (1965), and Dreitzler and Gross (1990) demonstrated that, instead of calculating the electron density from the many-electron wave function, one may work with the solutions to an effective one-electron problem (equation (21.8)). The method uses the form of the total-energy functional to identify an effective potential $V_{\mathrm{eff}}(r)$ as described above for one-electron states, and then to solve for the one-electron states to produce a density equal to the many-electron density. To account for the relativistic effects in actinides, it is necessary to replace the non-relativistic Schrödinger-like one-electron equation (equation (21.8)) by the relativistic Dirac equation. By finding the correct form for the effective potential, the electron density in equation (21.9) will be the same as that required by DFT.

The one-electron problem defined by equation (21.8) has the same form as the equations solved by band theorists before DFT was invented, and the eigenvalues of those equations as a function of crystal momentum are precisely the energy bands. The contribution of DFT is to provide a rigorous prescription for determining the new effective potential and for calculating the total ground-state energy, $E[n(\boldsymbol{r})]$.

The total energy functional within DFT is given by

$$E[n(\boldsymbol{r})] = T[n(\boldsymbol{r})] + E_{\mathrm{H}}[n(\boldsymbol{r})] + E_{\mathrm{xc}}[n(\boldsymbol{r})] + E_{\mathrm{eN}}[n(\boldsymbol{r})] + E_{\mathrm{NN}}, \tag{21.11}$$

where T is the effective kinetic energy of the one-electron states obtained from equation (21.9), E_{H} is the usual classical Hartree interaction between an electron and a charge cloud, E_{eN} is the interaction between an electron and nuclei, and E_{NN} is the inter-nuclear Coulomb interaction. The important term is E_{xc}, which is the one part of equation (21.11) that goes beyond the classical Hartree term obtained from the expression

$$E_{\mathrm{xc}}[n(\boldsymbol{r})] = \int n(\boldsymbol{r})\varepsilon_{\mathrm{xc}}(n(\boldsymbol{r}))\mathrm{d}\boldsymbol{r}. \tag{21.12}$$

This term represents the difference between the true energy of the eigenstates and the one-electron eigenstates. The operator of exchange-correlation $\varepsilon_{\mathrm{xc}}[n(\boldsymbol{r})]$ represents the sum of the exchange term $\varepsilon_{\mathrm{x}}(\boldsymbol{r})$ plus the correlation term $\varepsilon_{\mathrm{c}}(\boldsymbol{r})$.

The new (and presumably more correct) effective potential can now be obtained from the relationship

$$V_{\mathrm{eff}}(\boldsymbol{r}) = \delta/\delta n(\boldsymbol{r})[E_{\mathrm{H}}(n(\boldsymbol{r})) + E_{\mathrm{xc}}(n(\boldsymbol{r})) + E_{\mathrm{eN}}(n(\boldsymbol{r}))]. \tag{21.13}$$

With this new potential, the problem again reduces to a one-electron problem by substituting this potential into equation (21.8). From these definitions, it is clear that the effective potential in which the electron moves has contributions from the electron's interaction with the nuclei and the other electrons in the solid both by the classical Hartree term and by the quantum mechanical exchange and correlation terms.

Because all electron–electron interactions that go beyond the classical Hartree term are found in $E_{\mathrm{xc}}[n(\boldsymbol{r})]$, it is crucial to have a good approximation for this term. Unfortunately, there is no exact form of this term for a real solid. However, if one assumes the functional to be local, a numerical form may be obtained from many-body calculations (quantum Monte Carlo or perturbation series expansion), and very good values may be obtained for the ground-state energy for different values of the electron density. If the electron density of a real system varies smoothly in space, one expects that a form of E_{xc} taken from a uniform electron gas should be applicable to the real system as well. This approximation is none other than the LDA. The good agreement, for many solids, on cohesive energy, equilibrium volume, and structural properties between this approximate theoretical approach and experimental values suggests that the LDA form of E_{xc} works even if the electron density varies rapidly in space.

Thus, the total ground-state energy can be obtained by solving an effective one-electron equation. This tremendous simplification of replacing interacting electrons with effective one-electron states will work only if one can find the correct, effective one-electron potential. Good approximations can be obtained for $\varepsilon_{\mathrm{x}}(\boldsymbol{r})$ and $\varepsilon_{\mathrm{c}}(\boldsymbol{r})$ as determined by comparisons between the thus calculated band structures and experimental band structures measured by optical properties and photoelectron spectroscopy (PES).

21.4 GENERAL OBSERVATIONS OF 5f BANDS IN ACTINIDES

21.4.1 Narrow 5f bands

It is correct to say that the short radial extent of the 5f wave function yields only a small overlap between electrons from neighboring atoms and that this in turn results in very narrow 5f bands. Nevertheless, if the atomic spacing were sufficiently small, the overlap would be significant, as it is for 5f metals up to α-Pu. Why then does one not get a continuation of the actinide contraction (see Fig. 21.2) if the 5f electrons are involved in bonding?

Boring and Smith (2000) in their review argue that it is the presence of non-f bands at E_F (i.e. the 6p, 7s and to some extent the 6d bands), which contributes a repulsive force to the interatomic bonding forces (i.e. the s, p, d electrons with their larger radial extent, begin to repel each other at much larger distances). This is shown in Fig. 21.6 where the atomic-sphere approximation is used to calculate the contributions to bonding from individual bands for Pu (for

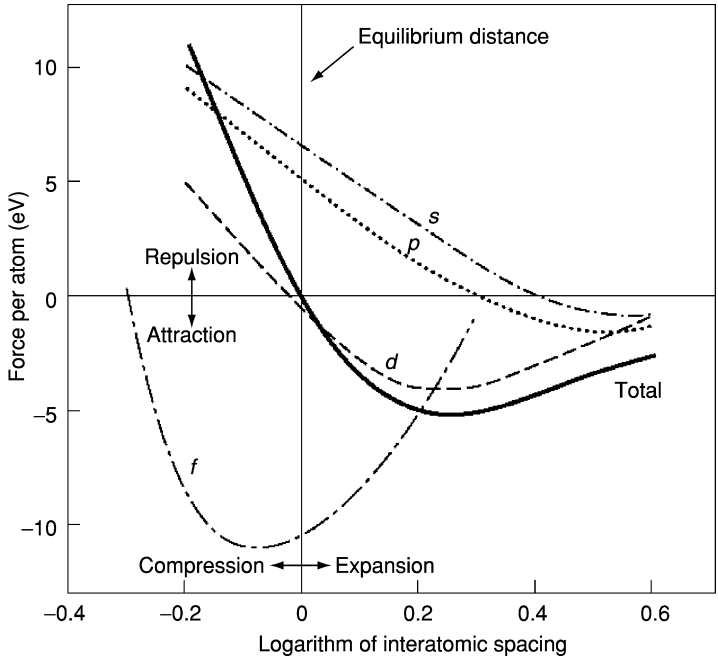

Fig. 21.6 *The force per atom as a function of interatomic spacing. DFT predictions for the bonding curves of δ-Pu in the fcc structure are plotted vs the interatomic spacing* $x = ln(a/a_0)$. *Included are the curve for the total cohesive energy per atom, and the individual contributions from the s, p, d, and f states. The f band is narrow at this larger volume* (*courtesy of Los Alamos Science*).

simplicity, in the fcc phase) as a function of interatomic spacing. For any single band, the calculated equilibrium spacing is that at which the interatomic forces on the atom are zero – i.e. where the calculated curve crosses the horizontal zero line.

From Fig. 21.6, one can see that if plutonium had only an f-band contribution, its equilibrium lattice constant would be smaller than that found. The f-band would be wider, and Pu would stabilize in a high-symmetry crystal structure. In reality, the contribution from the s–p band (a repulsive term at true equilibrium) helps to stabilize plutonium at a larger volume; the f-band is narrow at that larger volume, and the narrowness leads to the low-symmetry crystal structure. This argument is universal for multiband metals. In the transition metals, the s–p band is repulsive at equilibrium and leads to slightly larger volumes than would be the case if these metals had only d bands. For metals above Pu the repulsive force of the s–p bands is sufficient to prevent additional lattice contraction. The additional f-electron is no longer involved in bonding and it becomes energetically favorable for the entire f-subshell to localize. Another factor to the total energy balance is the correlation energy of electrons localized in atomic 5f states. The system gains the 5f bonding energy by the 5f delocalization, but as the electrons in atomic states can be better correlated than in band states, part of the correlation energy is lost.

In actinide compounds the whole range of narrow band behavior is observed, from transition-metal-like to localized. The existence of non-actinide atoms in compounds immediately yields a larger An–An separation so that a greater tendency toward localization is expected even in uranium compounds. This is in fact the case.

21.4.2 Low-symmetry structures from 5f bands

Fig. 21.3 shows a large number of low-symmetry crystal structures among the actinide metals. Actinide compounds, especially the more strongly correlated materials, show the same tendencies. It has long been assumed (at least for the pure metals) that it is the directional nature of the 5f bonds which leads to the low-symmetry structures. In recent years, the charge density for several actinides using the full-potential DFT method has been calculated. For elemental actinides up to Pu, no dominant directional 5f bonds have been found and, most importantly, no charge buildup between atoms (Söderlind *et al.*, 1995). What, then, is the driving force for the numerous transitions and low-symmetry allotropic phases? A general reason can be seen in the narrow 5f bands themselves. There exists a high density of 5f states at or near E_F so that a lowering of the electronic energy can occur through a Peierls-like distortion (Merrifield, 1966). The original Peierls distortion model was demonstrated in a one-dimensional lattice. It was shown that a row of perfectly spaced atoms can lower the total energy by forming pairs (or dimers). The lower symmetry causes the otherwise degenerate electronic energy levels to split, some becoming lower

Table 21.2 *Typical energies of the various interactions characterizing the localized picture of magnetism for ions with 3d, 5f or 4f unfilled shells.*

Interaction	3*d* (meV)	5*f* (meV)	4*f* (meV)
coulomb (U)	1000–10000	1000–10000	1000–10000
spin–orbit (Δ_{S-O})	10–100	300	100
crystal field (CF)	1000	100	10
exchange	100	10	1
bandwidth (W)	4000–10 000	700–5000	<500–2000

and others becoming higher in energy. The lowered levels are occupied by electrons, and therefore the distortion increases the bonding and lowers the total energy of the system. In the one-dimensional system, the distortion opens an energy gap at the Fermi level and makes the system an insulator. However, in the higher dimensional systems, the material can remain a metal in spite of the distortion because there are Bloch states from other bands that fill this gap.

In real three-dimensional lattices, the energy levels are degenerate along high-symmetry directions. If those levels lie close to E_F, a Peierls-like distortion of the crystal (i.e. a lowering of the symmetry) would increase the one-electron contribution to bonding, just as in the one-dimensional case described above. The Peierls mechanism is particularly effective if there are many degenerate levels near E_F, that is, if the energy bands are narrow, the DOS is large, and a large energy gain results from the distortion and filling of the lowered bands. Materials with broad bands (wider than 4 eV), gain less energy from level splitting because there are fewer levels near E_F. Indeed, symmetry-lowering distortions are rare in these materials. This is the dominant mechanism in cases where the energy is not lowered by other mechanisms removing part of the high-density states from the vicinity of E_F (magnetic ordering, superconductivity). In Table 21.2, a list of interaction energy ranges is given which highlights the types of interactions that are relevant in the actinides as well as the lanthanides and transition metals. The table shows Coulomb, spin–orbit, crystal field, exchange and bandwidth parameters. In the actinides, the large values and overlapping energy ranges for the interactions make the electronic structure calculations (and understanding) challenging.

21.4.3 The Hill plot

A very informative look at the effect of An–An spacing, and hence the effect of bandwidth, is provided in Fig. 21.7. This figure shows the transition temperatures for various uranium compounds, both magnetic and superconducting, plotted as a function of An–An spacing. Superconducting or magnetic-transition temperatures are plotted vertically, and the spacing between the f-electron elements is plotted horizontally. Hill first presented these results in the early

1970s (Hill, 1970) and found similar results for many different actinides and lanthanides. However, the presentation of data for uranium compounds yields much of the necessary information. Although some of this discussion pertains to magnetism, it is nevertheless presented here owing to its association with narrow 5f bands.

Fig. 21.7 shows that the crossover from itinerant to localized electrons can clearly be achieved if the actinide atoms are spread out. The most important aspect of Fig. 21.7 is the observation that a very limited number of magnetic uranium compounds are found with actinide spacing (in this case U–U) of less than about 3.4 Å. Inasmuch as magnetism is generally associated with more localized electrons, one may surmise that the 5f bandwidths for An–An separations smaller than 3.4 Å become too broad to support magnetism. Indeed, at these separations one may obtain direct f–f overlap. In Hill's initial plot, the known behaviors fell into only two of the four quadrants – large spacing correlated with magnetism and short spacing with superconductivity. Hill originally conjectured that the f-electrons could hybridize only with f-electrons at

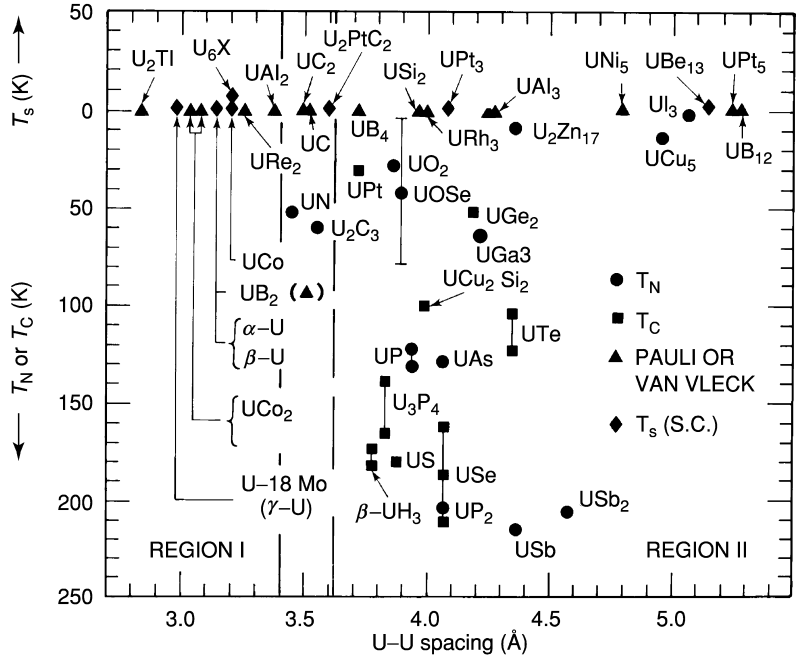

Fig. 21.7 *The 'Hill' plot for uranium compounds shows the interactinide spacing against a transition temperature (magnetic or superconducting). It is a general observation that magnetism is favored with the U–U spacing greater than 3.4Å while non-magnetic ground states are common below the separation. For uranium compounds, this distance roughly defines the localized/itinerant boundary for 5f states (after Hill, 1970).*

other sites and that the intervening non-f-electron atoms were just spacers to change the degree of overlap between the f-electron wave functions. Hill's plot became a major step toward understanding the light actinides, but it is now clear that the situation is more complex.

Fig. 21.7 depicts many more materials than were plotted in Hill's initial version. A large number of materials with large separations are now known to be non-magnetic. The existence of superconducting compounds is also found which, based on the relatively large distance between two f-electron atoms, should be magnetic. Two such compounds, namely, UPt_3 and UBe_{13}, are plotted in Fig. 21.7. They belong to a class of materials known as heavy-fermion superconductors first discovered in $CeCu_2Si_2$ (Steglich *et al.*, 1979) and later discovered in UBe_{13} (Ott *et al.*, 1983) and UPt_3 (Stewart *et al.*, 1984) setting off a period of intense research in heavy fermion and unconventional superconductivity research.

To understand the existence of non-magnetic compounds despite the large An–An separation, the concept of hybridization described in Section 21.3.3 above is utilized. It is not necessary to have direct f–f overlap of wave functions to produce relatively broad f-bands. Hybridization produces relatively wide f-bands that are broadened by the admixture of other symmetry components (the spd bands). It was shown by Koelling *et al.* (1985) that the lobes of the f-wave function allow the $AuCu_3$ simple cubic structure to be particularly amenable to hybridization with p- or d-bands along certain high-symmetry directions. Most materials having this structure are non-magnetic. Another observation is that for compounds in which the ligand atom contributes a high d-density at E_F, one generally obtains a strong f–d hybridization and a suppression of magnetism.

However, it is not true that the 5f-electrons are necessarily localized in compounds that are magnetic. Only one binary intermetallic compound (UPd_3) has been shown to exhibit true localized behavior of the 5f electrons. In nearly all other compounds, the hybridization with ligand sp bands is weak and leads to narrow band magnetism. In the case of extremely weak hybridization, one obtains the heavy-fermion compounds, among which those that have a superconducting transition (e.g. UPt_3 and UBe_{13} in Fig. 21.7) are very likely unconventional superconductors (Ott and Fisk, 1987).

21.5 STRONGLY HYBRIDIZED 5f BANDS

From the above Hill plot (Fig. 21.7), it is evident that many uranium compounds (and other actinide compounds also, particularly with Th and Pa, that are not shown in Fig. 21.7) have the characteristics of simple transition metals. This is true for the pure metals Th, Pa, and U as well (Np and α-Pu are questionable owing to a dearth of microscopic measurements). This class of materials is considered first. Because the pure metals are difficult to obtain in

single-crystal form, the compound UIr_3 will be considered as representative for this class of materials.

21.5.1 Fermi surface measurements in UIr_3

The $AuCu_3$-type compounds were perhaps the most extensively studied within the actinide group in the early years. They form readily (the phase often forms congruently from the melt and thus allows for very pure single crystals) which is just one more indication of strong bonding. UIr_3, like many of its isostructural materials, displays a large but temperature-independent paramagnetic susceptibility (of the order of 10^{-8} m^3/mol), thus indicating no localized magnetic moments. Its resistivity (linear with T at high temperatures) is of the order 20 $\mu\Omega$ cm at 300 K, which is again large but not when compared to Pu. It does, however, indicate that even in these relatively simple metals, one obtains some correlated electron behavior, not explained by the free-electron model.

In the 1970s, Koelling and coworkers calculated the electronic structure of UIr_3 as well as other U compounds using DFT, and found excellent agreement with experiment (see Arko *et al.*, 1985). Fig. 21.8 shows the measured de Haas–van Alphen frequencies (proportional to the extremal cross-sectional areas of the various pockets of the Fermi surface) for various directions of the magnetic field along symmetry lines. These are superimposed on dHvA frequencies calculated from the DFT band structure (solid lines) along the same symmetry directions. The agreement is phenomenal, especially when one considers that many of the refinements of DFT were not yet available in the early 1970s. Both the calculated Fermi surface volume and the topology are experimentally reproduced (Arko *et al.*, 1985).

It has been assumed that the Fermi surface remains unaltered in the presence of electron–electron correlations from what it would be in the absence of such interactions (Luttinger theorem; Luttinger, 1960). Thus, under this supposition, calculating the Fermi surface correctly is no proof of the validity of DFT. However, the Luttinger theorem states that only the Fermi surface volume is preserved, since the number of quasiparticle (defined below) states corresponds to the number of free-electron states. The topology, on the other hand, might be allowed to change if bands at the Fermi energy are altered by the interactions. Calculating the correct topology from DFT would suggest that the correlations are relatively weak and their effects have been included. In the case of UIr_3, this appears to be the case. This conclusion is reinforced by the observation that the measured m^* values do not exceed five times m_0. Recall that m^* is a rough measure of the electron–electron correlation strength.

21.5.2 Background on photoemission measurements

Since the dHvA effect only probes the states near E_F it is useful to consider other measurements that probe the electronic structure at higher binding energies. Perhaps the most direct such measurement is PES. In its simplest form this

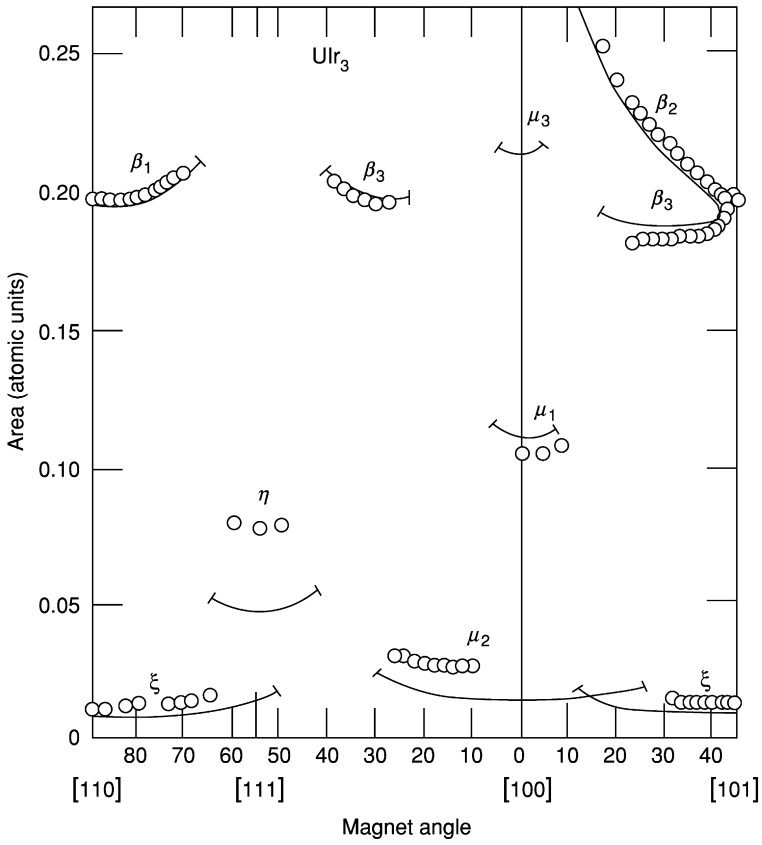

Fig. 21.8 *de Haas–van Alphen results indicating extremal areas for the Fermi surface of UIr_3. The open circles are the experimental data and the solid line is the DFT calculation. The agreement between experiment and theory is quite good over a large portion of the crystal structure* (*after Arko* et al., 1985).

measurement assumes that when an electron in quantum state $\boldsymbol{k}$ and energy eigenvalue E_k absorbs a photon and is ejected from the solid, the measured binding energy, E_B, is

$$E_B = E_{B,k} = -E_k \tag{21.14}$$

and the spectral function is a delta function at $E = -E_{kv}$ (i.e. absorption occurs at E_B and not elsewhere). This is referred to as Koopmans' theorem or the sudden approximation. For a non-interacting free-electron gas, this approximation seems reasonable. Even in the presence of small interactions, the above rule holds to a good approximation. However, in an interacting system, there occurs

a relaxation in the (N–1) electron solid and the relationship no longer holds. It becomes necessary to renormalize E_k by adding a correcting self-energy term $\Sigma(k,E)$ (Louie, 1992).

Assuming small corrections by measuring both the kinetic energy in vacuum, E_{Kin}, and angle θ of the outgoing electron (θ is measured relative to the surface normal), it is possible to determine both the energy and the momentum of the electron prior to the absorption of the photon; i.e. its energy state in the metal. The relationship is given by $E_{\mathrm{Kin}} = h\nu - E_{\mathrm{B}} - \phi$, where E_{Kin} is as above, $h\nu$ is the photon energy, E_{B} is the binding energy (or E_k) of the electron, and ϕ is the work function, or the energy lost in exiting the surface of the sample. The momentum components parallel and perpendicular to the sample surface are given by:

$$k_{||} = (\sqrt{2mE_{\mathrm{Kin}}})\sin(\theta), \quad \text{and} \quad k_{\perp} = (\sqrt{2mE_{\mathrm{Kin}}})\cos(\theta). \tag{21.15}$$

Since a photon does not change the direction of electron motion, the momentum information is preserved on photon absorption (so-called direct transitions). Indeed, as the electron exits through the sample surface, $k_{||}$ is preserved. An excellent reference for photoemission is the volume edited by Kevan (1992).

It is possible to determine electron momentum, $\boldsymbol{k}$, and map out the $E(\boldsymbol{k})$ vs $\boldsymbol{k}$ dispersion – i.e. the band structure by selectively sampling only electrons emitted in a narrow range of angles θ and measuring their energy. This is the so-called angle-resolved photoemission spectroscopy (ARPES). On the other hand, if the measurement accepts all electrons with a wide range of θ into the spectrometer, this will integrate over all momenta and yield, to a first approximation, the DOS. This is referred to as angle-integrated photoemission, or PES.

An important variation of PES is the so-called resonant photoemission. In simplified form, the data are taken at two photon energies: at the Fano resonance and at the Fano anti-resonance (Fano, 1961). The resonant energy roughly corresponds to a core level binding energy (in the case of U, $h\nu = 98$ eV, which is nearly the binding energy of the $5d_{5/2}$ core level). At this photon energy, the 5f photoemission cross section is greatly enhanced, while at the anti-resonance ($h\nu = 92$ eV for U), the 5f emission is strongly suppressed. By subtracting a PES spectrum taken at $h\nu = 92$ eV from one taken at $h\nu = 98$ eV one obtains the PES emission due to 5f electrons only. To a first approximation, this allows the measurement of the 5f DOS. Clearly this is a powerful tool. A fine reference for actinide photoemission is the chapter by Naegele *et al.*, (1985).

21.5.3 Photoemission in UIr_3

The ARPES measurements on UIr_3 is shown in Fig. 21.9 (Arko *et al.*, 1983). Most of the experimental data points ($E_{\mathrm{B},k}$) fall on top of the calculated bands, the notable exception being the experimental band labeled 'e' (see below). Since this data was obtained on a first generation synchrotron at 300 K with

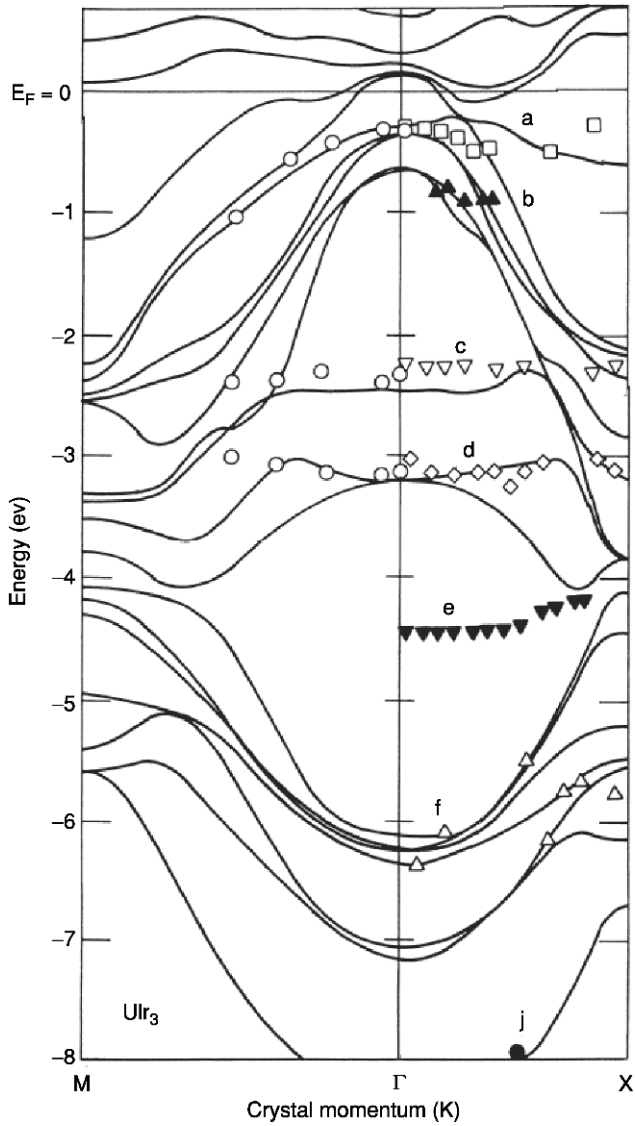

Fig. 21.9 *ARPES measurements and comparison to DFT calculations for* Uir_3. *The experimental data are the symbols and the calculation is represented by the solid lines. The agreement between experiment and theory is again quite good. The synergy between ARPES and DFT calculations is obvious in this comparison between the experimental and computational* E(**k**) *diagrams* (*after Arko* et al., 1983).

resolution no better than 200 meV, the agreement between experiment and theory is quite good. High-resolution low-temperature data would clear up the details at E_F, but from the data above the calculated bands at E_F are correct.

The 5f DOS is obtained by the resonance photoemission measurement described above (Arko *et al.*, 1983). Fig. 21.10 shows the calculated 5f DOS in UIr_3 as well as the measured result labeled 5f PES (dashed line). Although there appears to be a problem with intensity, it is necessary to consider that the 5f photoemission cross section varies with binding energy. If the 5f photoemission cross section is convoluted with the calculated 5f DOS, nearly perfect agreement with experiment is obtained. Thus UIr_3 (and the analogous compound URh_3) are simple band-like materials.

A vexing problem is band 'e' in Fig. 21.9, which has all the characteristics of a satellite. It is situated in a large gap in the calculated bands so that it is unlikely to be reproduced by DFT even with today's refinements. It was initially

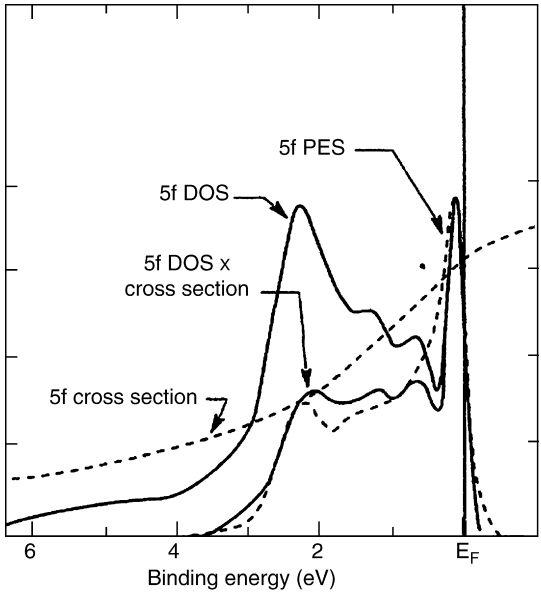

Fig. 21.10 *The calculated density of electronic states for UIr_3 compared against resonance photoemission. The resonance PES strongly enhances the 5f character in the spectrum. By separating the 5f component of the density of states in the DFT calculation, a direct comparison is made between experiment and theory. When the theoretical 5f DOS is modulated by the 5f cross section as a function of binding energy before comparison to the resonance photoemission, the results again show very good agreement between experiment and theory.*

attributed to Umklapp processes (translations by a reciprocal lattice vector, Arko *et al.*, 1985). While this may yet prove to be the case there is a possibility that it is due to correlations that are not contained within the DFT calculation. Band 'e' suggests that despite the general agreement with DFT, there is more to the story. It suggests electron correlation effects that are not strong enough to result in a renormalization of the band structure. While satellites are common in core level and atomic spectra, DFT is unable to account for such essentially final-state effects. By contrast, Fermi liquid theory, because of its different approach to weak correlations, yields a satellite as a natural consequence of the incoherent part of quasiparticle (see below) spectral weight (Kevan, 1992). Although band 'e' is not assigned to the incoherent part of the 5f spectral weight (it appears to be at a very high binding energy), this point is considered because of its applicability to more strongly correlated systems considered later.

21.6 WEAK CORRELATIONS – LANDAU FERMI LIQUID

Prior to the development of DFT, Landau (1957) argued that electrons in the conduction band act as if they were nearly free even though the individual electrons are subject to strong Coulomb forces. Landau's idea was based on the effect of the electrons' correlated motions from mutual interactions in the solid. The electrons tend to 'clothe' themselves, so as to screen their charge (the details are complex and involve the entire system). These 'clothed' electrons were called 'quasiparticles'. Based on properties of strongly interacting electrons at the Fermi level, Landau showed that the system of strongly interacting electrons can be remapped onto a system of weakly interacting quasiparticles, which preserve some characteristics of electrons such as spin, momentum, and charge, while other quantities like the mass are renormalized. The consequence is that expressions known from weakly interacting electrons and describing temperature dependences of magnetic susceptibility, electrical resistivity, and specific heat preserve the same analytical form, while only prefactors are renormalized by the interactions. In mathematical terms, E_k is renormalized, as above, so that $E_k^1 = E_k^0 + \Sigma(k, E)$, where E_k^0 is the free particle eigenvalue, and $\Sigma(k,E)$ is the self-energy term with real and imaginary components. For the weakly interacting Fermi liquid, $\Sigma(k,E)$ can be parameterized in the form

$$\Sigma(k, E) = \alpha E + \mathrm{i}\beta E^2 \tag{21.16}$$

The general effect of $\Sigma(k,E)$ on photoemission (see Kevan, 1992 for a complete derivation) is to yield a spectral function (for E_k^1) consisting of a coherent part called the quasiparticle peak, and an incoherent part which can, in a loose fashion, be associated with a satellite resulting from a relaxation of the (N–1) particle system. A schematic of such a spectral function is shown in

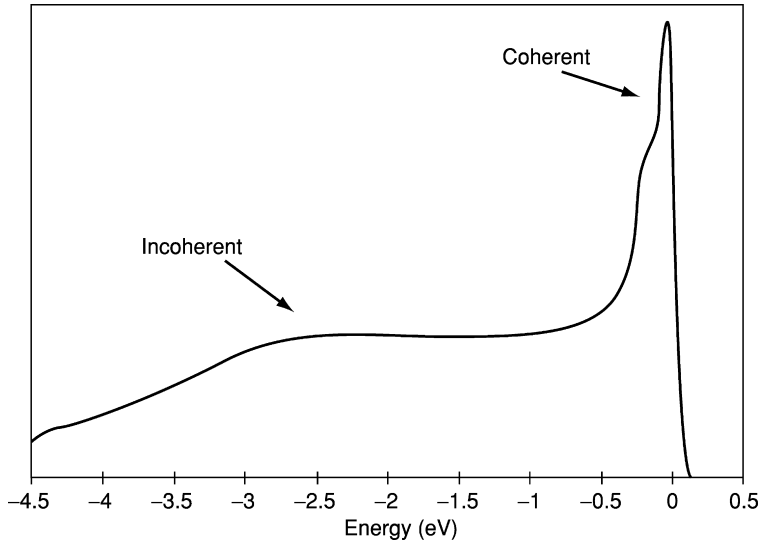

Fig. 21.11 *A schematic representation of a photoemission spectrum within a correlated electron description of the system. The coherent portion of the spectrum would represent the well-defined quasiparticle character described by Landau's Fermi liquid theory, and the incoherent portion would represent emission not consistent with such well-defined quasiparticles. The self-energy which contains all of the interactions beyond the one-electron picture may represent both a shift in energy and a broadening from the one-electron states.*

Fig. 21.11. In atomic spectra such satellites are referred to a shake-up satellites. The strength of the incoherent peak increases with increasing interaction strength. For the weakly interacting Fermi liquid it can be shown that the coherent part of E_{k}^{1} (the position of the quasiparticle peak) is given by

$$E_k^1 = E_k^0(1-\alpha)^{-1}. \tag{21.17}$$

The resolution at E_{F} in Fig. 21.9 is insufficient to draw conclusions regarding E_{k}^{1}, but it is possible that the very weak band "e" can be associated with the incoherent part of E_{k}^{1}.

It is useful to look at the signature that a Fermi liquid has on electrical resistivity. The net effect of the correlations is to contribute a quadratic temperature term to the resistivity at low temperatures; i.e., $\rho(T) = aT^2$ where a is a constant. If the interaction is sufficiently strong, this term, due to electron–electron interactions, will dominate over the weak T^5 term at very low temperatures. At higher temperatures, of course, the usual linear term may be expected. Fig. 21.12 shows plots of resistivity vs temperature for several actinide

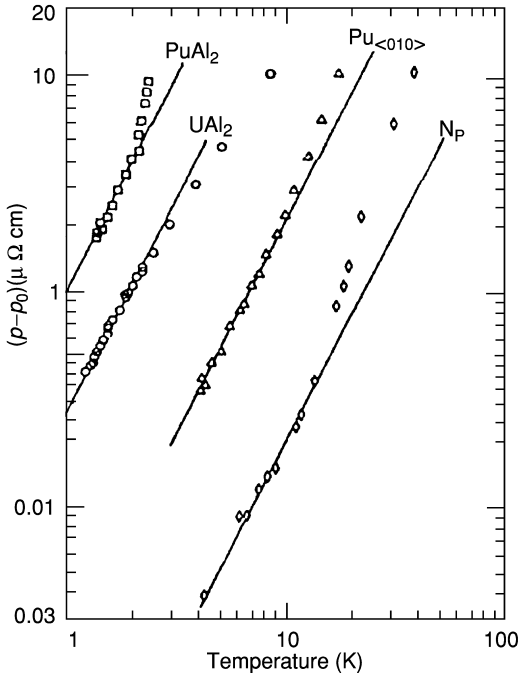

Fig. 21.12 *Resistivity for Np, Pu, $PuAl_2$, and UAl_2 as a function of temperature. The T^2 dependence of the resistivity clearly places these materials in the Fermi liquid category of metals. At higher temperatures, additional effects beyond the electronic contributions begin to have a substantial role in the resistivity* (*after Arko* et al., 1972).

systems where clearly the T^2 term is dominant. The T^2 term persists in strongly correlated systems so that all compounds are considered Fermi liquids if they display a T^2 rise in resistivity at low temperatures.

21.7 STRONG CORRELATIONS

21.7.1 Heavy fermions

Perhaps the most interesting compounds in the actinide series are the so-called heavy-fermion compounds. In general, these are very narrow band materials on the verge of localization whose conduction 5f electrons behave as if they had an extremely heavy effective mass. Indeed they blur the distinction between itinerant and localized states, making it seem as if there was a continuous transition. Fully localized electrons, with their definite energy levels, can be thought of as belonging to an infinitely narrow band and having an infinite effective mass

since they are unable to travel beyond the bounds of their atomic site. The effective masses of heavy-fermion materials, by contrast, range from tens to hundreds of times the mass of a typical itinerant electron in normal metals, indicating a very low but finite velocity through the crystal.

The unusual collective ground states of heavy fermions arise from very strong electron correlations involving the electrons in their narrow bands, and their low-energy excitations are associated with the spin and charge fluctuations in that narrow band. Of the light-actinide metals, only δ-Pu might be associated with heavy-fermion behavior, and even here there is room for debate. It is the large An–An separation in compounds that results in the narrow bands, particularly when hybridization is weak. Recent experiments on the phonon dispersions by inelastic X-ray scattering for delta phase Pu (Wong *et al.*, 2003) demonstrate the unique nature of Pu and the complex interactions involving electron-phonon coupling in this material.

Heavy-fermion behavior was first discovered in Ce compounds having one 4f electron; in particular, $CeCu_2Si_2$. Despite their magnetic susceptibility that at high temperatures suggested magnetic behavior, the susceptibility became temperature-independent at the low-T end and the material exhibited a superconducting transition with an extremely large specific heat anomaly. Subsequently similar behavior was observed in materials having 5f electrons, initially UPt_3 and UBe_{13}. This was most unusual since it was assumed that nearly localized electrons cannot even conduct electricity, much less support superconductivity. It slowly became clear that a new ground state of matter existed, one in which electron interactions were so highly correlated that only an extreme quasiparticle picture could cause that behavior. More specialized information on heavy fermion (both actinide and anomalous lanthanide) systems can be found in reviews of Grewe and Steglich (1991) and Nieuwenhuys (1995).

The unusual bulk properties of UBe_{13} are displayed in Fig. 21.13. The behavior of specific heat C_P at low temperatures, particularly the extremely large C_P/T ratio (in normal metals it is of the order 1 mJ mol^{-1} K^{-2}) points to an m^* perhaps on the order of 1000 and is also reflected in the large superconducting anomaly. Note that the low-temperature state of heavy fermions can be superconducting, antiferromagnetic, or simply paramagnetic. In all cases, however, as shown for UBe_{13} in Fig. 21.13, the magnetic susceptibility (plotted as $1/\chi$ in Fig. 21.13) exhibits Curie–Weiss behavior at high temperatures, but then levels off or even decreases at low temperatures. The upper critical field is extremely high, reaching a value of 6 T at 0.4 K. A most unusual property is the electrical resistivity, ρ, which has a negative temperature dependence down to about 10 K, and then drops precipitously.

Although there remains disagreement as to the nature of this ground state, the most widely accepted model is the so-called single impurity model (SIM). The origins of the SIM stem from the theory used for transition metal impurities in a noble metal matrix, a true impurity scenario. The model was extended to f-electron systems and later to situations where the 'impurity' nature of the

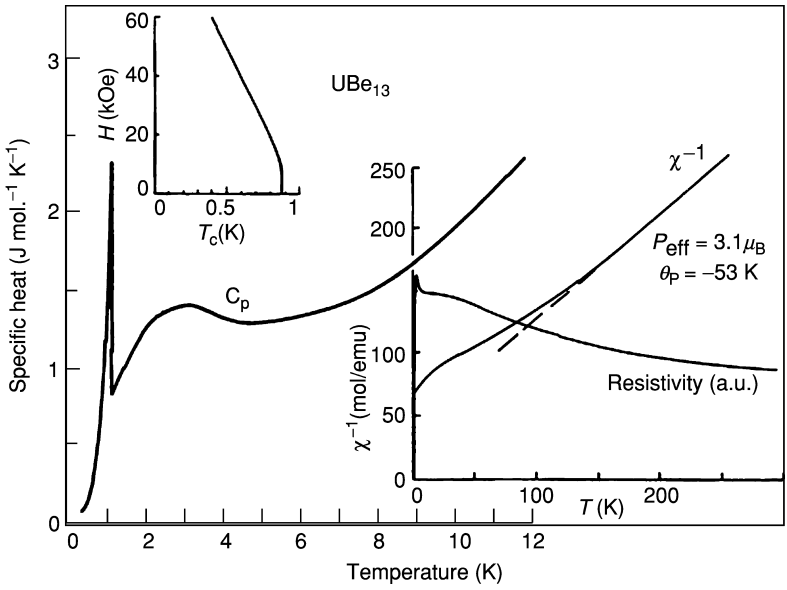

Fig. 21.13 *The thermodynamic properties (magnetic susceptibility, specific heat, and magnetic field dependence of* T_C*) of the heavy-fermion–superconductor* UBe_{13} *are plotted against temperature. The superconducting transition just below* 1 K *is clear from the specific heat while the anomalous resistivity and susceptibility for a metal are plotted on a much larger temperature scale showing the heavy-fermion nature of* UBe_{13} *(after Fisk* et al.*,* 1985).

problem was far exceeded. This model presumably strictly applies to Ce compounds having only one f-electron, but the similarities of properties in all heavy fermions suggest that one model might qualitatively apply to all. Attempts to compensate for the SIM shortcomings in the area of periodicity have given rise to extensions of the original idea in a periodic array with the Kondo lattice and Anderson lattice being two such models. A more detailed description of these models and predictions may be found in Arko *et al.* (1999). The description given here is for completeness and due to the lack of a more comprehensive model.

Within the SIM picture, the 4f or 5f electrons behave at high temperatures as if they were localized magnetic impurities at binding energy ε_f (sometimes called the bare f-level), having no interaction with each other or non-f electrons. As the temperature is lowered, however, they do hybridize slightly with the remaining non-f conduction electrons via a Kondo-like interaction whereby the conduction electrons align antiparallel to the f spin in order to screen the magnetic moment. The hybridization strength Δ is generally small. When the moment is fully screened, the susceptibility becomes independent of T. At still lower temperatures, this cloud of conduction electrons, which through hybridization has acquired a small amount of f-character, forms a coherent

ordered array (Kondo and Anderson lattice models) and a very narrow f-band at the Fermi energy. The amount of f-character at the Fermi energy is $(1-n_f)$ where n_f is nearly unity and represents the f-character remaining in the localized f-state at ε_f – the bare f-level. Essentially, $\Delta(1-n_f)$ is the probability that a conduction electron will occupy an already occupied f-level. A very loosely defined characteristic temperature, the Kondo temperature or $T_K = \Delta(1-n_f)/k_B$, approximates the onset of coherence. Indeed, most properties of heavy fermions in principle scale with T_K.

The SIM more or less successfully explains the bulk properties shown in Fig. 21.13. The heavy mass arises from the screening cloud and associated spin fluctuations, the negative $\rho(T)$ from the scattering from localized impurity moments, and the precipitous drop in ρ is due to coherence. However, there are numerous unresolved problems even for Ce compounds, among which is the fact that the approximations of SIM are only valid for n_f near unity (Arko *et al.*, 1999), whereas n_f values as low as 0.5 have been erroneously ascribed to heavy fermions.

Since the bare 5f-level, essential to SIM, has never been clearly observed in actinide compounds, Fig. 21.14 portrays instead photoelectron spectra of $CeBe_{13}$, having a T_K of 400 K in order to elucidate some of the problems. The near-E_F peak in the figure has been associated with the f-density acquired by the conduction electrons (the Kondo resonance), while the feature near −2.5 eV has been associated with the bare f peak. Despite its crucial importance to the validity of SIM, an unconventional temperature dependence has never been established for the near-E_F peak. The problem remains unresolved in large part due to the difficulty of the measurement and is outside the scope of this chapter. Instead the focus is on only one of the many discrepancies with SIM, namely the $\boldsymbol{k}$-dependence of the bare f-peak evident in the figure between the (100) and the (110) directions. This is totally inconsistent with the concept of a localized state.

While the SIM appears to capture some of the physics associated with bulk properties, its failure to incorporate periodicity causes it to fail the test of microscopic measurements. Newer models such as the periodic Anderson model (PAM) or the dynamical mean-field theory (DMFT) (Savrasov *et al.*, 2001) do incorporate the f-electron periodicity and show some promise, though the calculations are extremely difficult. It is useful to also point out that in the mid-1990s, Bedell and his coworkers developed very simplified one- and two-band Fermi liquid models of heavy-fermion compounds such as UPt_3 (Sanchez-Castro and Bedell, 1993). The surprise was that these simplified models yielded quantitative results in agreement with the low-energy and low-temperature physics of these materials. This is presented here because the dispersing bare-f level of Fig. 21.14, while totally inconsistent with SIM, is consistent with Landau's incoherent state. It would appear that Landau's principle of one-to-one correspondence between electron and quasiparticle states continues to have validity and yields profound insights into systems of strongly interacting particles.

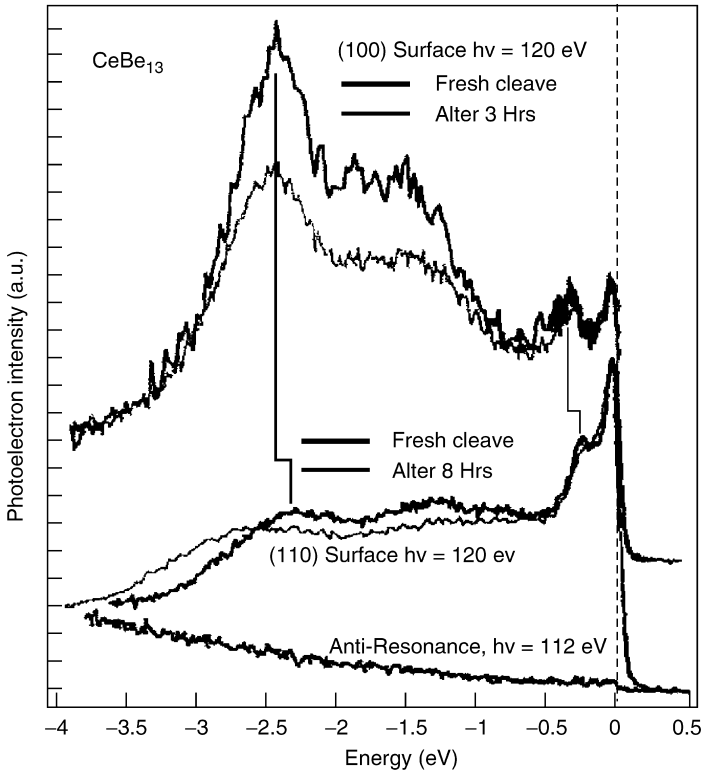

Fig. 21.14 *Resonance photoemission data for the enhanced mass compound $CeBe_{13}$ with a characteristic temperature of 400* K. *The PES data show two crystallographic orientations which demonstrate major variations in the electronic structure of the material, particularly the 5f levels, as a function of position in reciprocal space. The dotted vertical line at the zero of binding energy is the Fermi level. The peaks centered between* 2 *and* 2.5 eV *below the Fermi energy are attributed to the 'bare' f^0 peak in Kondo-type description of the system. The data are presented for freshly cleaned samples and three hour old samples in order to assess the role of surface features in the electronic structure* (*after Arko* et al., 1999).

21.7.2 Special case of plutonium systems

Plutonium and its compounds appear to present ground states different from heavy fermions or predictions from DFT-derived band structure calculations. Even α-Pu, which has been considered a relatively ordinary transition-metal-like system based on the ability to correctly calculate its atomic volume, does not yield PES results consistent with DFT calculations. All phases in the ordered state, however, conform to the requirements of a Fermi liquid as shown in Fig. 21.12. While the resistivities of both α-Pu and δ-Pu closely resemble resistivities of heavy fermions (see Fig. 21.15), the magnetic susceptibilities are

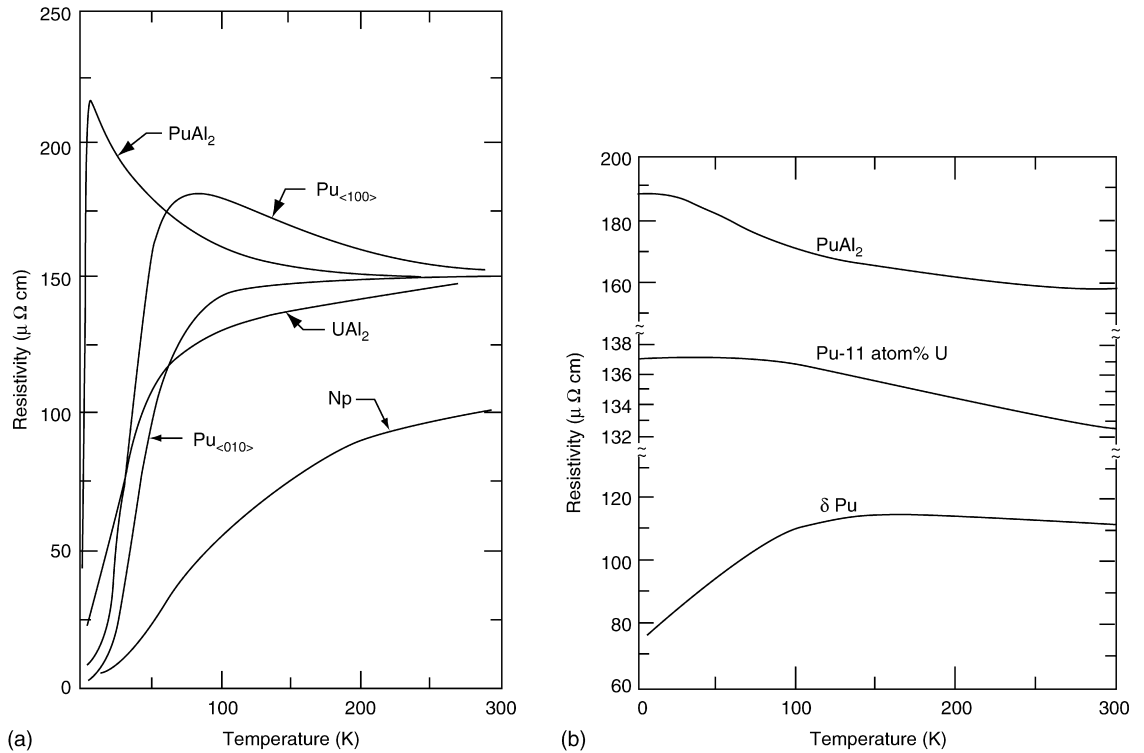

Fig. 21.15 *Electrical resistivity as a function of temperature for $PuAl_2$ and other actinides. The role of disorder and radiation are manifest in the resistivity. The difference in the low-temperature resistivity for $PuAl_2$ in (a) and (b) is a result of radiation damage. A similar effect may be generated by alloying where the impurities disrupt the integrity of the lattice as seen in (b). Separating intrinsic many-body phenomena such as quantum criticality from radiation and impurity effects is an ongoing challenge in actinide metals, alloys, and compounds (after Arko* et al., 1972).

temperature-independent, albeit large (of the order of 10^{-9} m^3 mol^{-1}). The specific heat γ-values are 17 and ≈ 64 mJ/mol. K^2 for α- and δ-Pu, respectively, which places them near the bottom of the range for heavy fermions (Lashley *et al.*, 2003). Eriksson *et al.* (1999) took a novel approach to the Pu problem and explored the localization of an integral fraction of the 5f electrons in δ-Pu in their DFT calculation (actually, the generalized gradient approximation or GGA, which extends LDA), while allowing other 5f electrons to be itinerant and involved in bonding. This is the mixed-level model (Eriksson *et al.*, 1999; Wills *et al.*, 2004). Using this technique, they were able to correctly calculate the atomic volume of δ-Pu, as well as obtain agreement with PES spectra (Joyce *et al.*, 2004). Indeed, the same approach appears to work for several other Pu compounds as well (Joyce *et al.*, 2003). This computational scheme provides an understanding of the 5f electronic structure as consisting of 5f electrons both in a localized as well as in an itinerant configuration for Pu, which is the cross-over point in the actinide series between localized and itinerant f-electron characteristics. The concept of the 5f electrons having a dual nature is not unique to Pu metal or its intermetallic compounds. This approach of separating the 5f character into localized and itinerant can also be found in insulating Pu oxides and other actinide systems (Petit *et al.*, 2003), the magnetically mediated, heavy-fermion superconductor UPd_2Al_3 (Sato *et al.*, 2001) and for the original actinide heavy-fermion superconductor UPt_3 (Zwicknagl and Fulde, 2003). For the δ-phase of Pu metal, the dual nature of the 5f electrons was initially proposed by Joyce *et al.* (1998). In Fig. 21.16 the energies are calculated for localized and itinerant 5f electrons for U, Pu, and Am. Clearly, an itinerant 5f framework is appropriate for U and just as clearly, a localized model is the choice for Am. In the boundary region of Pu, the energy level for localized and itinerant 5f character are nearly degenerate, and thus this mixed level character in Pu and Pu-based compounds would not be surprising.

An alternative interpretation for Pu PES results was considered (Gouder *et al.*, 2000; Havela *et al.*, 2002, 2003). The fact that a number of Pu-based systems show similar characteristic narrow features in the range 0–1 eV below E_F led to a conjecture that details of particular band structure are not dominant in this energy range. Instead final-state effects, either a fingerprint of atomic-state multiplet (whose high-energy lying states can be seen due to the excitation at the photoemission process) in analogy to 4f systems, or a general structure originating from many-electron process, are responsible for the observed structures (Fig. 21.17). It is interesting that the 5f states tend to localize in ultra-thin layers, as the reduced mean number of nearest neighbors leads to a preference for nonbonding 5f states. Calculations based on a DMFT may yield better agreement in the future, but these calculations at this point are in the early stages (see Savrasov *et al.*, 2001).

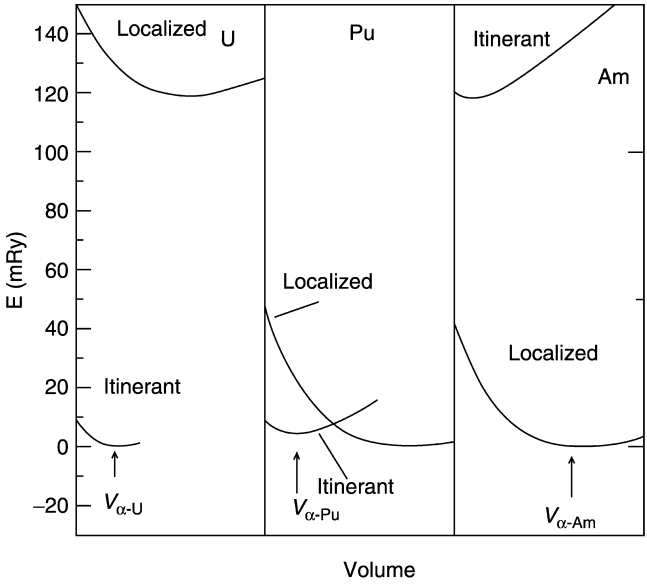

Fig. 21.16 *Total energy vs metallic radius (volume) for uranium, plutonium, and americium treating the 5f electrons as either localized or itinerant. For uranium, the calculation strongly favors an itinerant character to the 5f levels while for americium the localized 5f character is favored. Plutonium sits at the boundary between localized and itinerant. The boundary position of Pu supports the mixed-level approach to treating Pu 5f electrons (after Wills and Eriksson,* 2000).

21.7.3 Non-Fermi liquid effects and the quantum critical point

Actinide metals and most of their associated compounds typically follow the Fermi liquid scaling of electrical resistivity and electronic specific heat. Their respective coefficients reach the strongly renormalized (enhanced) values for narrow 5f-band systems. This contrasts with the systems with broad 5f-bands on one side and magnetic materials with sizeable moments on the other side, where the respective coefficients reach smaller values. The latter case deals with correlations of non-f electrons only. But some compounds persistently fail to meet the Fermi liquid rules at all. While the Fermi liquid concept requires resistivity to increase from zero temperature with a T^2 dependence, in such anomalous cases the value of the exponent can be lower. Instead of the normal constant value for C/T, logarithmically increasing C/T values with decreasing T are found. Such behavior can be encountered in the vicinity of the onset of magnetic ordering, in particular, if the parameters of the system are tuned so that its critical temperature for magnetic ordering reaches the $T = 0$ K limit. In such a situation, thermal fluctuations are suppressed and quantum fluctuations start to dominate.

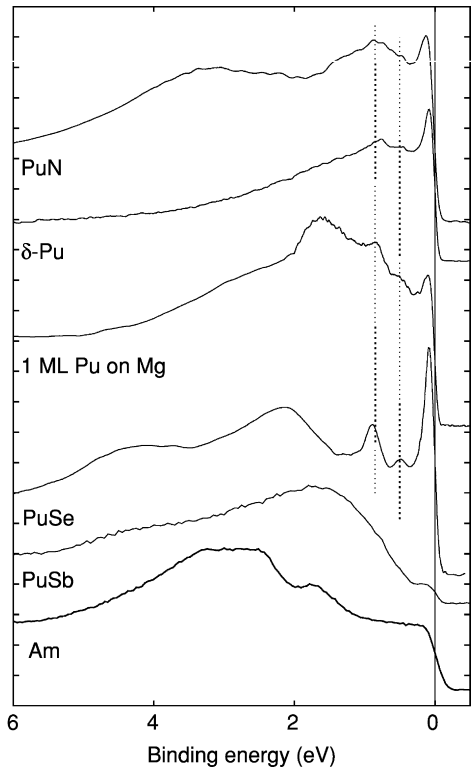

Fig. 21.17 *Examples of UPS valence-band spectra* ($h\nu = 40.8$ eV) *of selected Pu systems and Am demonstrate the effect of the* 5*f localization* (*in Am and PuSb*), *which reduces the spectral intensity at the Fermi level* (E = 0). *More itinerant Pu systems* (*PuN, δ-Pu, PuSe*) *exhibit a high spectral intensity at* E_F, *while a variable fraction of the localized* 5*f states is observed* 1–3 eV *below* E_F. *The latter dominates also for one monolayer of Pu on Mg. The dotted lines indicate positions of rather generally occurring features, which do not belong to particular DFT electronic states.* (*Reprinted with permission from Havela* et al., 2003.)

Unfortunately, efforts to bring a system to this so-called quantum critical point by the proper doping of impurities into the system also results in a randomness in the structure due to the statistical occupation of atomic positions. In most instances of non-Fermi liquid (NFL) behavior, the explanation has been one of disorder. Fig. 21.15a shows the resistivities of $PuAl_2$ and other materials whose low-temperature resistivity has been shown to vary as T^2 in Fig. 21.12. Upon disorder (via self-damage by α-particles), the resistivity of $PuAl_2$ in Fig. 21.15b no longer drops at low temperatures, but rather seems to level off. Only about 1% of the sample is estimated to sustain disorder caused by damage from α-particle bombardment during 1 month of shelf time, assuming that no room temperature annealing occurred. This shows how little disorder it takes

to destroy coherence in very narrow bands. The resistivity of Fig. 21.15a can be entirely reproduced by annealing the specimen at 1000°C for 12 h (Arko *et al.*, 1973).

One of the microscopic models accounting for the NFL behavior in such inhomogeneous systems is based on a distribution of Kondo temperatures T_K due to the atomic disorder. Numerous such systems include $(U,Y)Pd_3$, $U(Cu,Pd)_5$, or $(U,Th)Ru_2Si_2$. A summary of NFL features in actinides and lanthanides can be found in Stewart (2001). Sometimes NFL scaling is observed even in undoped systems. Undoubtedly in such a case the sample has the real characteristics of strongly correlated systems. Approximate theories indicate several fundamental classes of NFL behavior (instead of one class of FL scaling) which depend on the character of magnetic interactions (ferro- or antiferromagnetic) and on dimensionality (for example f-sites may form weakly interacting sheets or chains, thus reducing the effective dimensionality). These parameters determine the degrees of freedom of the quantum fluctuations, which affect the type of analytical behavior describing basic quantities. For example, in the proximity of three-dimensional ferromagnetism, the characteristics $\rho \sim T^n$, $n = 5/3$ and $C/T \sim -\ln(T/T_0)$ are expected. For antiferromagnetic coupling, the n value is reduced to 3/2 and further reduction takes place for lower dimensionality. In the two-dimensional case, $n = 4/3$ and 1 for the ferromagnetic and antiferromagnetic coupling, respectively. Although the majority of undoped NFL systems are found among Ce or Yb intermetallics, there are also a few U-based intermetallics. For example, at ambient pressure, NFL features are observed in UCoAl, U_2Co_2Sn, or U_2Pt_2In. The review article by Stewart (2001) describes these and other examples.

21.8 CONVENTIONAL AND UNCONVENTIONAL SUPERCONDUCTIVITY

Superconductivity, with its basic characteristic of the complete disappearance of electrical resistivity at low temperatures, has been traditionally considered as a contradiction to magnetic ordering. The reason is related to the Cooper pairs, consisting of two electrons with opposite momentum and spin, which are the basic ingredient of the superconducting state (Bardeen *et al.*, 1957). Indeed, a very small admixture of magnetic ions into a normal superconductor rapidly suppresses the superconductivity, and this phenomenon has to be attributed to the breaking of such electron pairs by exchange interactions, which prefer a parallel orientation of electron spins.

This conventional superconductivity is commonly found in actinides that are only weakly magnetic, although the critical temperatures T_c are very low. For example, $T_c = 1.37$ K for Th (Gordon *et al.*, 1966), 1.4 K for Pa (Fowler *et al.*, 1965), and 0.68 K for α-U (Hein *et al.*, 1957). For heavier actinides, superconductivity was found for Am ($T_c = 0.79$ K) (Smith and Haire, 1978). Similarly, intermetallic compounds with high actinide content also tend toward

superconductivity. The highest T_c values are found in compounds of the form U_6T, where T = Mn, Fe, Co, Ni, reaching the highest $T_c = 3.7$ K for U_6Fe, and U_3Ir ($T_c = 1.24$). Several others, U_3Si, U_3Os, U_2Ti, all have T_c below 1 K (see Sechovsky and Havela, 1988 and references therein). The same is true for amorphous U-rich systems (metallic glasses) (Poon *et al.*, 1985), while similar Th-based systems (e.g. $Th_{80}Co_{20}$) reach T_c at nearly 4 K. For lower U content, a tendency to magnetic ordering appears and superconductivity ceases. But this is not universally the case. A strange island of superconductivity was discovered for some compounds with a high inter-uranium spacing, which have characteristics close to a normal magnetic ordering (UBe_{13}, UPt_3, see above). (Ott and Fisk, 1987). Some variations of these compounds even order antiferromagnetically and the magnetic order and superconductivity coexist. In this case of so-called unconventional superconductivity, the pairing mechanism of the Cooper pairs is related to magnetic interactions instead of the electron–phonon coupling of normal Cooper pairs (Bardeen *et al.*, 1957) in the BCS mechanism. Here the superconducting state may be based on electrons with parallel spins (as opposed to antiparallel) with the total wave function therefore having a different symmetry. This phenomenon is called d-wave or p-wave symmetry in contrast to the s-wave symmetry in conventional BCS superconductivity. Such superconductors can be strongly anisotropic, including the anisotropy of the superconducting gap, and the superconducting state also can be much more resistant against a magnetic field (Ott and Fisk, 1987). The intimate connection of the superconductivity and the heavy-fermion character of the electronic structure is manifest in the huge jump of the specific heat C, scaling with γT_c. This scaling strongly suggests that the heavy-fermion character and the superconductivity are related to the same set of 5f electrons.

The most prominent materials among unconventional superconductors were already mentioned in the Heavy Fermion section. In the first of these, UBe_{13}, T_c can reach 0.85–0.90 K, and is very dependent on the actual purity of the sample (Ott and Fisk, 1987). This compound is of particular interest by virtue of its enormous γ ($\gamma = 1100$ mJ mol^{-1}K^{-2} and it is one of the U compounds with the most 'heavy' electrons) and its strongly anomalous resistivity in the normal state, increasing with decreasing T towards a sharp maximum at $T = 2.5$ K. It was first assumed to be non-magnetic, but very small static magnetic moments of $0.001\mu_B$ were deduced from muon spin-relaxation studies (Heffner *et al.*, 1990). The very high upper critical field $B_{c2} = 9$ T (considering the low T_c value) is consistent with the unconventional nature of the superconductivity.

UPt_3 with $\gamma = 420$ mJ mol^{-1} K^{-2} can be also classified as a heavy-fermion superconductor. The superconducting transition temperature again depends strongly on the sample quality. A T_c of 0.53 K can be obtained in well-annealed samples (Franse *et al.*, 1984). Unlike UBe_{13}, UPt_3 displays well-documented antiferromagnetic correlations, shown by neutron scattering experiments. An unusual static magnetic order with very low magnetic moments develops below about 5 K (Aeppli *et al.*, 1988).

Superconductivity (T_c = 0.8 K) and antiferromagnetism (T_N = 17.5 K) coexist also in URu_2Si_2, which has only a moderate γ value (75 mJ mol^{-1} K^{-2}) (Maple *et al.*, 1986). Although ordered magnetic moments do not exceed $0.04\mu_B$/U where μ_B is the Bohr magneton, the specific heat anomaly at T_N and the total entropy related to magnetic ordering is so large that there appeared numerous speculations about other type of ordering (e.g. quadrupolar), invisible to the neutron diffraction, which could induce a secondary weak magnetic ordering. The search for this so-called hidden order is still in progress (see for example Chandra *et al.*, 2002). An alternative approach, based on dynamic long-range correlations carrying a large magnetic entropy, has been proposed (Bernhoeft *et al.*, 2003).

Even larger ordered moments and higher superconducting transition temperatures are found in the superconducting antiferromagnets UPd_2Al_3 and UNi_2Al_3. UPd_2Al_3 has a higher ordered moment $(0.85 \pm 0.03)\mu_B$/U and ordering temperature of 14.4 K (Krimmel *et al.*, 1993). Unlike the Néel temperature, the superconducting critical temperature is strongly sample dependent, varying with a slight off-stoichiometry and/or heat treatment of single crystalline samples between 1.5 and 2.0 K. An interplay of superconductivity and magnetic fluctuations revealed by inelastic neutron scattering (Bernhoeft *et al.*, 1998) indicates importance of magnetic interactions in the unconventional superconductivity mechanism. UNi_2Al_3 orders antiferromagnetically below $T_N = 4.5$ K and the magnetic order coexists with superconductivity below $T_c \approx 1$ K (Geibel *et al.*, 1991), γ reaches 140 and 120 mJ mol^{-1} K^{-2} for the Pd and Ni compounds, respectively.

All these compounds are very exotic, but even more surprising was the recent discovery of the ferromagnetic superconductors UGe_2 and URhGe. The superconductivity in UGe_2 appears only in a state induced by high pressure. Although high pressure finally led to the suppression of magnetism, at pressures around 12 GPa, where the superconducting temperature reaches its maximum (about 0.7 K), the magnetization still corresponded to about $0.8\mu_B$/U with the Curie temperature at about 30 K. The superconductivity disappeared in fields of several tesla, where a high-magnetization state was induced in a first-order magnetic phase transition. An overview of the data on this compound as well as on URhGe is given in Flouquet *et al.* (2003). On the other hand, URhGe is already superconducting at ambient pressure. Its critical temperature reaches only 0.3 K ($T_c = 9.5$ K), with U moments around $0.4\mu_B$/U.

The most recent breakthrough in the superconductivity of actinides was the discovery of Pu-based nearly magnetic systems with superconductivity in the temperature range exceeding 18 K (Sarrao *et al.*, 2002). The fact is surprising because $PuCoGa_5$ is the first known Pu superconductor. The Ce-based isostructural compounds $CeCoIn_5$, and $CeIrIn_5$ are superconducting also, but only in the 1 K range, and for $CeRhIn_5$ only under pressure. The high γ value of $PuCoGa_5$, 77 mJ mol^{-1} K^{-2} points to strong electron–electron correlations. This value, and the high estimated upper critical field 74 T, is indicative of

an unconventional superconductivity. The T_c of $PuCoGa_5$ can be further enhanced to about 22 K by applying pressure (Griveau *et al.*, 2004). $PuRhGa_5$ is superconducting, as well, with $T_c = 8.6$ K (Bauer *et al.*, 2004).

21.9 MAGNETISM IN ACTINIDES

The peculiar character of the electronic structure of actinides, with the 5f states ranging between localized and itinerant, implies an extreme variability of magnetic features of elemental actinides as well as actinide-based alloys and intermetallic compounds. The gradual filling of the 5f shell in the sequence of actinide elements does not dominate the development of the magnetic properties of the pure elements in the way expected on the basis of parallel lanthanide series. This is especially true for the early actinides, in which a 5f band is formed, as described in Sections 21.3 and 21.4. Therefore more similarity is found with the d transition metals, exhibiting broad s and p bands and narrow d bands. As a consequence, the density of electronic states at the Fermi level, $N(E_F)$, is a more important parameter than the filling of the 5f band itself. The interactinide spacing has a crucial role. For pure elements, it is too small, and substantial 5f–5f overlap leads to a rather broad 5f band and weak magnetic behavior.

For heavier actinides (from Am onwards) the 5f localization was documented for the pure elements, and atomic correlations in analogy to rare earths leads to the formation of local moments and their ordering. At closer inspection, specific features of band magnetism appear in systems based on elements up to Pu. The main characteristics of the 5f band magnetism comprise strong spin–orbit interaction, leading to large orbital moments formed even in the case of band-like states, exchange interactions mediated or assisted by the hybridization of the 5f states with the ligand states, and enormous magnetic anisotropy arising from the anisotropy of the hybridization (bonding anisotropy). Another characteristic is a high sensitivity of magnetic properties to external variables, like pressure, magnetic field, and to fine details of composition. More detailed information can be found in review chapters (Sechovský and Havela, 1988, 1998). Electronic structure calculations based on the density functional approach are discussed by Johansson and Brooks (1993) and by Norman and Koelling (1993). The impact of magnetism on transport properties for actinides and lanthanides are compared by Fournier and Gratz (1993).

21.9.1 General features of magnetism of light-actinide systems

The fundamental difference between the character of the 4f electron states in lanthanides and the 5f states in light actinides can be attributed to a much larger spatial extent of the 5f wave functions, and thus a much stronger interaction with their metallic environment, compared to the 4f case. The 5f electrons are, as

a rule, delocalized due to their participation in bonding, which leads to a considerable hybridization of the 5f states with the valence states of neighboring atoms (5f-ligand hybridization). The delocalization of the 5f electrons has serious consequences, such as the formation of a more or less narrow 5f band intersected by the Fermi energy E_F (the bandwidth W_{5f} is of the order of several eV) rather than discrete energy levels. Consequently, the magnetic moments due to the itinerant 5f electrons are much smaller than expected for a free ion (irrespective whether the L–S or j–j coupling schemes are used – ground state magnetic moments are similar), and magnetic moments can disappear in a broadband limit leading to weak temperature-independent (Pauli) paramagnetism. This situation resembles to a certain extent the 3d transition metals. The strength of magnetic coupling in cases of existing 5f moments is typically much larger than for the 4f moments interacting via the Ruderman–Kittel–Kasuya–Yosida (RKKY) interaction, which is reflected by higher ordering temperatures compared to isostructural rare earth systems. The impact on magnetic excitations is even more dramatic, no crystal-field excitations can be observed by inelastic neutron scattering in the vast majority of systems studied so far, but a rather broad quasielastic response reflecting the 5f-moments instability in analogy to, for example, cerium mixed valence materials is observed (Holland-Moritz and Lander, 1994).

21.9.2 Magnetism in pure An elements

A small separation between the ions of the pure elements leads to large overlap of the 5f wave functions of nearest neighbors, amounting to the formation of a broad 5f band and weakly paramagnetic behavior. With increasing 5f occupation, the value of the Pauli-type susceptibility increases due to the increase of $N(E_F)$, the DOSs at the Fermi level, which is corroborated by a similar increase in the low-temperature electronic specific heat coefficient γ (see Table 21.1). This tendency is interrupted between Pu and Am, where the 5f states localize, and do not contribute to bonding for heavier actinides. The reason for the localization (and loss of the 5f bonding energy) can be found qualitatively in the gain of electron correlation energy for atomic-like 5f states (which is partly lost in the 5f band case). For details, see Johansson and Brooks (1993).

Quantitatively, the lack of magnetic ordering can be deduced from the Stoner criterion, which specifies conditions for magnetic ordering in band systems. If the Stoner product $U^*N(E_F)$, which contains besides the DOS at the Fermi level the intra-atomic Coulomb interaction parameter U, is larger than 1, the spin-up and spin-down sub-bands are not occupied equally and net magnetization arises. For light-actinide metals, this criterion is not fulfilled and the sub-bands are not split. Light-actinide metals can lower their electron energies by forming different open crystal structures, sometimes of a very low symmetry (in analogy to Jahn–Teller effect). The best example of this phenomenon is Pu having six allotropes, with the ground-state allotrope, α-Pu, showing a

complicated monoclinic structure. A similar situation is found in α-U, the structure of which is orthorhombic, but an incommensurate charge-density wave is formed below $T = 43$ K (Lander *et al.*, 1994). Due to the weakly magnetic character, superconductivity can appear at the beginning of the actinide series, as mentioned earlier.

Plutonium, the element on the verge of localization, exhibits the most complex behavior. Its room temperature phase, α-Pu, is monoclinic with 16 atoms per unit cell. At $T = 388$ K, it undergoes a phase transition to an even more complicated monoclinic β-phase with 34 atoms per unit cell. For remaining phases, most of data exists on the fcc δ-phase with four atoms per unit cell, which has atomic volume expanded by 26% compared to the α-phase, and which can be stabilized by several percent doping with Al, Ce, Ga, or other trivalent elements. Comparing the fcc δ-phase to the data for α-Pu given in Table 21.1, γ is strongly enhanced to (64 ± 3) mJ mol^{-1} K^{-2} (Lashley *et al.*, 2003). It is an interesting fact that all the Pu phases have only a small difference in magnetic susceptibility (see Table 21.1). The highest value was recorded for the β-phase, which also exhibits a noticeable temperature dependence in the narrow temperature range of its existence (Olsen *et al.*, 1992). The most surprising is the lack of magnetic order in the δ-phase with the largest atomic volume. LDA or GGA calculations invariably lead to a magnetic state, with spin and orbital moments only partially canceling each other (Söderlind and Sadigh, 2004). Méot-Reymond and Fournier (1996) discussed the properties of δ-Pu in terms of a Kondo effect (i.e. many-electron effect based on dynamical screening of a local atomic spin by spins of conduction electrons) with the characteristic Kondo temperature T_K higher than room temperature. Also Savrasov *et al.* (2001) suspect dynamic phenomena, described by a DMFT, to wash out magnetism. Another conjecture trying to solve the δ-Pu puzzle is the idea that there are magnetic moments in δ-Pu, but they are disordered, not leading to a long-range order (Niklasson *et al.*, 2003). But as the low δ-Pu susceptibility is quite robust with respect to various dopings or even lattice expansion (Hecker *et al.*, 2004 and references therein), it seems that it is fundamentally non-magnetic. Such non-magnetic character ($S = 0$, $L = 0$) could be obtained using an LDA+U method, where U denotes an explicit involvement of intra-atomic coulomb correlations going beyond LDA (Shick *et al.*, 2005) but this approach needs to be reconciled with the photoemission and the enhanced mass results. Such calculations suggest that the 5f count in δ-Pu is about 5.5, and is not only much higher than typically 5.0 in α-Pu, but relatively close to the non-magnetic $5f^6$ configuration.

The elements beyond Pu behave rather similarly to the lanthanide series. The analogy starts with the crystal structures. Am, Cm, Bk, and Cf all have dhcp structures, but the structures change and the 5f states delocalize under external pressure, yielding low-symmetry structures of the light-actinides type (Lindbaum *et al.*, 2003). The non-magnetic ground state of Am (exhibiting a low value of γ and quite high Van Vleck susceptibility) can be understood in the

framework of either L–S or j–j coupling for the $5f^6$ configuration. Most of information on curium (Cm) was obtained on the ^{244}Cm isotope (half-life 18 years), which is available in large amounts (milligrams) but displays high self-heating and radiation damage. A maximum in the magnetic susceptibility indicating antiferromagnetic (AF) ordering was observed at $T = 52$ K for this isotope, and a simple antiferromagnetic order was indeed confirmed by neutron diffraction. For ^{248}Cm, which has a longer half-life of 340,000 years, but is available only in small amounts, the antiferromagnetic ordering occurred at $T = 64$ K. Values of effective moment are compatible with $\mu_{\text{eff}} = 7.55\mu_{\text{B}}$ expected for the intermediate coupling model. Besides the ground-state dhcp crystal structure, a high-temperature fcc phase can occur in a low-temperature metastable state. Its magnetic ordering temperature is enhanced to $T = 205$ K. Berkelium (Bk) and californium (Cf) can be studied only in sub-milligram quantities. For Bk, antiferromagnetic ordering was deduced below $T = 34$ K. Cf is probably ferromagnetic below approximately 51 K. Both materials display μ_{eff} values compatible with free-ion theoretical values in the paramagnetic state. Einsteinium, which can be studied in sub-microgram quantities only, yields a moment of $11.3\mu_{\text{B}}$, which is even somewhat higher than the theoretical value. For more detailed information on magnetism of transplutonium actinides, see the review of Huray and Nave (1987) and references therein.

21.9.3 Magnetic properties of actinide intermetallic compounds

Similar to pure actinide elements, the magnetic properties of intermetallic compounds reflect the gradual filling of the incomplete 5f-shell. In Th compounds, the very small filling of the 5f states cannot give rise to the 5f magnetic moments, and compounds are typically Pauli paramagnets with susceptibility χ_0 of the order of 10^{-9} to 10^{-8} m^3 mol^{-1} for intermetallic compounds, indicating a low DOS at E_{F}. The ground state is frequently superconducting (Sechovsky and Havela, 1988). Exceptions are compounds such as Th_2Fe_{17} ($T_{\text{C}} = 295$ K) and Th_2Co_{17} ($T_{\text{C}} = 1035$ K), in which the magnetism is dominated by transition-metal components (Buschow, 1971).

In the compounds of U, Np, and Pu magnetic ordering can appear when the actinide–actinide spacing is enhanced to such an extent that the 5f-band narrowing and consequent increase of the DOS at E_{F} leads to the fulfillment of the Stoner criterion. The proximity of these elements to the boundary between the localized and itinerant character of the 5f-electronic states makes them very sensitive to variations of the environment. In the first approximation, the width of the 5f band can be taken as a function of the overlap of the 5f atomic wave functions centered on nearest neighbors, and the increase of the overlap can be taken as the principal delocalizing mechanism of the 5f electrons. The prominence of the Hill limit, introduced earlier (see Fig. 21.7), is evident. The situation is best documented for U compounds, where the Hill distance $d_{\text{U–U}} = 3.4$–3.6 Å is an approximate boundary value of the spacing, corresponding to the critical

5f–5f overlap. For smaller spacing values, most of the compounds are non-magnetic (often superconducting), for d_{U-U} larger than the Hill limit, the compounds usually show a magnetically ordered ground state. The value of the Hill limit should be taken as very approximative, the width of the 5f band is naturally affected also by the coordination number.

For compounds with d_{U-U} larger than the Hill limit, the principal control parameter is not the U–U spacing, but the hybridization of the 5f states with electronic states of other components. In particular, in compounds with transition metals, it is mainly the overlap of the 5f states with the d-states of the transition metal that affects the strength of the hybridization. The 5f states remain pinned at the Fermi level in most cases, whereas the late transition metals (as well as noble metals) being much more electronegative have their particular d states shifted towards higher binding energies thus leaving the 5f–d overlap small on the energy scale. The reduced 5f–d hybridization leads to the onset of the 5f magnetism, whereas the d-states are occupied more than in the pure d-element. Even if the d-element itself is magnetically ordered (Co, Ni, Fe), in the compound with U, it behaves as essentially non-magnetic (a similar effect appears in Th compounds). Exceptions are compounds with very high content of the transition metal component, in which case the d-magnetism can prevail. In compounds with the earlier d-metals like Fe or Ru, the d-states appear closer to the Fermi energy and the 5f–d overlap increases, leading typically to a non-magnetic ground state (as in UFeAl). But in some cases, magnetic moments appear both on the U and transition-metal ions. Prominent examples are Laves phases with Fe, all ordering ferromagnetically. Relatively high T_C values (UFe_2, 162 K; $NpFe_2$, 492 K; $PuFe_2$, 564 K;, $AmFe_2$, 613 K) point to the dominance of Fe–sublattice exchange interactions, but actinide magnetic moments are non-negligible, reaching $1.1\mu_B$/Np or $0.45\mu_B$/Pu. The tiny total moment in the case of U is caused by the orbital ($0.23\mu_B$) and spin ($0.22\mu_B$) components nearly canceling each other (Sechovsky and Havela, 1988 and references therein).

In compounds with non-transition metals, it is mainly the size of ligand atoms that affects the hybridization. Compounds with larger ligands are typically magnetic (e.g. UIn_3), whereas those with smaller ligands and greater hybridization form broad bands with low $N(E_F)$ and are weakly paramagnetic (USi_3). Several characteristic groups of U compounds can be thus distinguished.

(a) Compounds with very high U content

The stoichiometry leads to a small U spacing, d_{U-U}. The consequence is a broad 5f band similar to U metal. These compounds are weakly paramagnetic and superconducting. The examples, U_6Fe, U_6Co, U_6Ni, U_3Ir, U_3Si, U_3Os, and U_2Ti were mentioned in the section on superconductivity. The lower U concentration compound, which can be classified as a regular superconductor with moderate $d_{U-U} = 3.2$ Å, UCo has $T_C = 1.22$ K (Chen *et al.*, 1985).

(b) Lower U content, small $d_{U—U}$ much below the Hill limit

This stoichiometry leads to a weakly paramagnetic behavior, possibly with an influence of spin fluctuations, and the ground state is not superconducting. As examples, one may give U_3Si_2, UAl_2, or UCo_2. The last two compounds belong to an extended group of so-called Laves phases, which combine atoms of two different sizes into a very closely packed cubic or hexagonal structure. Therefore although the U content is relatively low, the packing leads to $d_{U–U}$ much below the Hill limit. Some of these compounds do not undergo magnetic ordering, also partly due to the strong hybridization of the 5f states with the d-state of transition metal constituents (UMn_2, UCo_2, URe_2). But the Laves phases with Fe and Ni are ferromagnets, and belong therefore to the next group (Sechovsky and Havela, 1988 and references therein).

(c) Itinerant ferromagnets with $d_{U—U}$ around or below the Hill limit, 3.4 Å

When proceeding from the most U-rich compounds and decreasing the U concentration, one observes magnetic order (ferromagnetism) at the 1:1 stoichiometry. Typical examples have very small ordered moments and relatively high ordering temperatures (UIr: $T_C = 46$ K, spontaneous magnetic moment $\mu_s = 0.45\mu_B$). For UNi_2, the very small spontaneous moment $0.08\mu_B$/U led to the conjecture that the magnetism was due to a small fraction of Ni atoms occupying wrong crystallographic positions (Franse *et al.*, 1981). But neutron diffraction proved finally that magnetism was not carried by Ni, but by U, and what is observed in the magnetization is a small difference between the orbital and spin moments with antiparallel orientation (Fournier *et al.*, 1986). UFe_2, the first U compound for which magnetic ordering was reported (Gordon, 1949), is a somewhat different case. Fe atoms carry magnetic moments (although much reduced by the hybridization compared to Fe metal) and lead to a high Curie temperature $T_C = 162$ K. The nearly complete mutual cancellation of spin and orbital moments reduces the contribution of U to the total magnetization to practically zero, but polarized neutron diffraction can accurately detect both components (for details, see Sechovsky and Havela, 1988).

Focusing thus on the sequence of the U-3d Laves phases, an interesting non-monotonic development of magnetism is observed. UMn_2 is non-magnetic and strongly hybridized, as the 5f and 3d bands have a strong energy overlap, and this situation does not allow the formation of Mn or U moments. In UFe_2, the 3d states shift towards somewhat higher binding energies, but the hybridization with the 5f states, given by the energy overlap, remains strong. The Fe sublattice orders ferromagnetically, allowing for the formation of the U moments. In UCo_2, the 3d band shifts even deeper and is close to filling. The Fermi level is in a minimum between the 3d and 5f states, therefore magnetism is lost again. For UNi_2, the 3d band is filled, the Fermi level is on the ascending

edge of the 5f band, and the Stoner criterion leads to magnetism of purely 5f origin (Eriksson *et al.*, 1989).

(d) Low U concentration, large $d_{U—U}$, ferromagnetic ground state

Ferromagnetism appears typically for uranium compounds with a moderate U–U spacing. For higher spacing, ferromagnetism changes to antiferromagnetism due to a more indirect exchange interaction. The ferromagnet with the highest d_{U-U} (among known binaries) is UGa_2 (shortest d_{U-U} in UGa_2 is 4.01 Å). It exhibits a sizeable spontaneous moment of $2.7\mu_B$/U and a rather high $T_C = 126$ K (Andreev *et al.*, 1979). As γ is only about 5 mJ mol^{-1} K^{-2} (Ballou, 1983), it was often assumed to form 5f localized states, but both the decreasing magnetization under pressure and microscopic (PES) data point to the itinerant character (Reihl *et al.*, 1985; Gouder *et al.*, 2001). Another prominent representative of this group is UGe_2 ($T_C = 52$ K, $\mu_s = 1.43\mu_B$/U), mentioned in the context of unconventional superconductivity, which was observed under pressure (Saxena *et al.*, 2000).

(e) Compounds with a very low U concentration

Within this group, the U—U spacing is significantly over the Hill limit, and consequently the direct 5f–5f overlap becomes insignificant. The strength of the 5f–ligand hybridization determines whether the ground state is magnetic or non-magnetic. This can be well demonstrated for the series UT_3 where T is a transition metal and UX_3 with X a p-metal, all sharing the $AuCu_3$ cubic structure type. For UX_3, the relation of the hybridization and the radius of the p metal can be found. For large X-radii, the falloff of the wave functions of the X-ligand at the U atom is generally small, and the hybridization is weak. For small X ligands, the spatial variations of their wave functions are larger and the hybridization is stronger (Koelling *et al.*, 1985). The crossover from weak Pauli paramagnetism to magnetic ordering occurs as X gets heavier, where X represents elements from the columns of the periodic table with p^1 and p^2 states. Thus USi_3, UGe_3, and UAl_3 are weak paramagnets, USn_3 still shows non-magnetic spin fluctuations, whereas UGa_3, UPb_3, UIn_3 and UTl_3 are antiferromagnets. The highest ordering temperature $T_N = 95$ K was found in UIn_3. In the group of UT_3 compounds, magnetic ordering depends mainly on the strength of the 5f–d hybridization, modulated by the overlap of the two types of states determined by the energy scale (Koelling *et al.*, 1985). It is generally reduced for T at the end of transition-metal series, as the d band shifts below the Fermi level, whereas the 5f states stay pinned at E_F. The development is similar to that in the Laves phases, but no d-originating magnetism is found in this group. UCo_3, URu_3, URh_3, and UIr_3 are weak paramagnets, nearly magnetic UPt_3 (heavy-fermion superconductor) and UPd_3 with localized $5f^2$ states and a quadrupolar ordering have a different structure type. UPd_3 is thus an interesting reference case; no

other binary compound exhibits the f-states shifted from the Fermi level (shown by PES; see Baer, 1984). Also neutron scattering experiments reveal well-defined crystal-field (CF) excitations (Buyers and Holden, 1985; McEwen *et al.*, 1993), normally absent in the spectra of uranium intermetallics, and γ reaches only 5 mJ mol^{-1} K^{-2} (Andres *et al.*, 1978). Compounds with high concentrations of a transition element can exhibit also high-temperature magnetic ordering. For example, ferromagnetic order with a high Curie temperature (360 K) in $UCo_{5.3}$, studied by Deryagin and Andreev (1978), is undoubtedly related to Co.

(f) Heavy-fermion materials

The last group comprises those having a substantially enhanced γ-coefficient of the specific heat and show a coexistence of magnetic ordering and superconductivity of an unconventional type. If these materials undergo a magnetic ordering, the critical temperatures are very low. Typical examples are UCu_5 ($T_N = 15$ K), U_2Zn_{17} ($T_N = 9.7$ K), UCd_{11} ($T_N = 5$ K), and the heavy-fermion superconductor UBe_{13}. For details, see Ott and Fisk (1987) and references therein.

(g) Other compounds

Besides binary compounds, there exist large groups of ternary compounds, often including a transition metal T and a non-transition metal X (UTX, U_2T_2X, UT_2X_2), which follow the tendencies of the 5f-ligand hybridization mentioned above. The advantage of studies of the *5*f magnetism in such compounds is that both the transition and non-transition metal components can be varied, while the structure type, i.e. the symmetry of environment of actinide atoms, is preserved. Thus the crossover from a non-magnetic to a magnetic ground state can be studied in more detail.

Materials, which are in the boundary region (i.e. nearly or weakly magnetic), show a variety of so-called spin-fluctuation features. Those with a non-magnetic ground state exhibit Curie–Weiss behavior of the magnetic susceptibility at high temperatures, but at low temperatures, a broad maximum in $\chi(T)$ appears (e.g. URuAl, UCoAl), other types of spin fluctuations are characterized by a plateau in $\chi(T)$ below a characteristic temperature, and then a low-temperature upturn as found in URuGa (Sechovsky and Havela, 1998). High ordering temperatures can be achieved with ternary compounds, for example, in compounds of the $UT_{10}Si_2$-type ($ThMn_{12}$ structure type), in which both the U and transition metal T (Fe, Co) carry magnetic moments. The highest $T_C = 750$ K was recorded for $U(Fe_{0.5}Co_{0.5})_{10}Si_2$ (Berlureau *et al.*, 1991).

The occurrence of magnetic ordering in Np-based compounds is dominated by mechanisms analogous to their U-counterparts. Important information is obtained using the ^{237}Np Mössbauer spectroscopy, which can determine microscopic parameters of the Np magnetism such as the magnetic hyperfine field B_{hf} on the Np nucleus. Values were found approximately proportional to the local

Np magnetic moment μ_{Np} (Dunlap and Kalvius, 1985; Potzel *et al.*, 1993): $B_{hf}/\mu_{Np} = 215$ (T/μ_B). The boundary between the magnetic and non-magnetic behavior for different Np materials is not much different than for their U-isotypes and demonstrates that for Np compounds, the mechanisms of the 5f-delocalization play a comparable role. Thus the non-magnetic behavior of Np in $NpGe_3$ and $NpRh_3$ has to be attributed to the 5f–p and 5f–d hybridization in analogy to UGe_3 and URh_3 (Sechovsky and Havela, 1988 and references therein). On the other hand, differences also exist. For example, $NpSn_3$ is an itinerant antiferromagnet, whereas USn_3 shows spin-fluctuations not undergoing magnetic ordering. Such a difference can be generally attributed to a higher 5f count or weaker 5f delocalization. On the other hand, Np_2Rh_2Sn is a non-magnetic spin fluctuator, whereas U_2Rh_2Sn undergoes antiferromagnetic order ($T_N = 24$ K) (Sechovsky and Havela, 1998). Moreover, ^{237}Np Mössbauer spectroscopy under high pressure has been a convenient tool to distinguish different types of magnetically ordered compounds. For those with more stable 5f moments, the Np moment does not decrease with pressure in the GPa range while the ordering temperature increases (e.g. $NpCo_2Si_2$), whereas a pronounced decrease of both parameters points to a stronger 5f-moment instability, e.g. as in Np Laves phases $NpOs_2$ or $NpAl_2$ (Potzel *et al.*, 1993 and references therein).

For intermetallic compounds of Pu, two tendencies cross each other. One is a stronger tendency to 5f localization due to the proximity of the Pu–Am borderline. On the other hand, the tendency to magnetism is diminished by small free-ion magnetic moments of the $5f^5$ state in both L–S and j–j coupling schemes. For $5f^6$, the moment is zero. For example, $PuMn_2$ is a weak paramagnet (although $NpMn_2$ is a ferromagnet), and a similar situation is found for the couples $NpCo_2$–$PuCo_2$ and $NpNi_2$–$PuNi_2$, and $NpRe_2$–$PuRe_2$. The Pu compounds that order magnetically include $PuRh_2$ ($T_N = 10$ K), $PuFe_2$ ($T_C = 564$ K, due to the ferromagnetism of the iron sublattice), $PuPt_3$ ($T_N = 40$ K), $PuPd_3$ ($T_N = 24$ K), $PuRh_3$ ($T_N = 6.6$ K). The knowledge of magnetism of Am intermetallics is fragmentary. The ferromagnetism of $AmFe_2$ ($T_C = 613$ K) is explained by the properties of the Fe sublattice. $AmRh_2$ is a paramagnet. For details, see Sechovsky and Havela (1988).

21.9.4 Magnetic properties of other actinide compounds

A large majority of actinide compounds even with non-metallic elements have metallic character. The magnetic behavior is dominated by the f–p hybridization, which has a dual role. It leads both to a delocalization of the 5f states and mediates the exchange interaction. The metallic character appears in most of the rocksalt-type of compounds, monopnictides AnX (An = U, Np, Pu, X = P, As, Sb, Bi) and monochalcogenides AnY (An = U, Np, Y = S, Se, Te), which are magnetically ordered and reach appreciable temperatures for the magnetic phase transition, as, for example, $T_N = 213$ K in USb or 285 K in UBi. On the other hand, Pu monochalcogenides are semimetallic and

non-magnetic (for details, see Vogt and Mattenberger, 1993). Carbides, which are of slightly under-stoichiometric ratios (AnC_{1-x}) are weakly magnetic for An =Th, Pa, U. NpC_{1-x} is ferromagnetic below $T = 225$ K, whereas antiferromagnetic ordering is found up to about 300 K, depending on the x values. PuC_{1-x} undergoes antiferromagnetic ordering with T_N ranging between 100 and 30 K, depending on the stoichiometry (Fournier and Troc, 1985). A large data set exists for nitrides AnN. Whereas ThN and AmN are weakly magnetic, magnetic ordering appears for UN ($T_N = 53$ K), NpN ($T_C \approx 90$ K), presumably also in PuN ($T_N = 13$ K), in CmN ($T_C = 109$ K), and data exist even for BkN ($T_C = 88$ K). For other compounds, high-temperature magnetic ordering can be found, for example, in U_3As_4 ($T_C = 196$ K), U_3Sb_4 ($T_C = 146$ K), or even 400 K for antiferromagnetic ordering in U_2N_2As. USb_2 and UAs_2 are antiferromagnets with $T_N = 205$ and 273 K, respectively (Fournier and Troc, 1985). The magnetism of actinide dioxides is covered in Chapter 18.

U forms a trihydride with hydrogen known to be a ferromagnet ($T_C = 180$ K). antiferromagnetic order was found in PuH_2 ($T_N = 30$ K), whereas PuH_3 is ferromagnetic ($T_C = 101$ K) (Aldred *et al.*, 1979) Np hydrides are weakly paramagnetic, which can be understood as due to crystal field effects for the $5f^4$ ionic state (Aldred *et al.*, 1979). For a review covering hydrides, see Wiesinger and Hilscher (1991). Hydrogen can be absorbed also by a number of binary and ternary intermetallic compounds. Similar to elemental light actinides, it strongly supports the tendency to form local 5f magnetic moments and order magnetically, which can be at least be partly attributed to the 5f-band narrowing due to enhanced inter-actinide spacing. Actinide compounds with non-metallic components are, together with discussions of general aspects of actinide compounds, covered in the review of Fournier and Troc (1985). Properties of systems containing boron are covered by Rogl (1991).

21.9.5 Orbital moments in light actinides

Although the majority of light actinides and their intermetallic compounds are characterized by itinerant 5f-states, an important difference with 3d magnetics is in the energy of the spin–orbit coupling Δ_{S-O} and the width of the 3d (5f) band W_{3d} (W_{5f}). Whereas $\Delta_{S-O} << W_{3d}$, their respective values in light actinides become comparable because Δ_{S-O}(5f) is of the order of eV. The relevant energy scales are indicated in Table 21.2. Due to the strong spin–orbit interaction, typically a large orbital magnetic moment μ_L is induced. It is antiparallel to the spin moment for U, in analogy with light lanthanides and the third Hund's rule stating that the total angular momentum is given by $J = L–S$ for the first half of the series. The existence of such orbital moments for the 5f-band systems was revealed first from band structure calculations involving a spin–orbit interaction term coupling the spin and orbital moment densities. Experimentally it was confirmed by the studies of the neutron form-factor, which adopts a very specific shape with a maximum, especially if the spin and orbital moments are

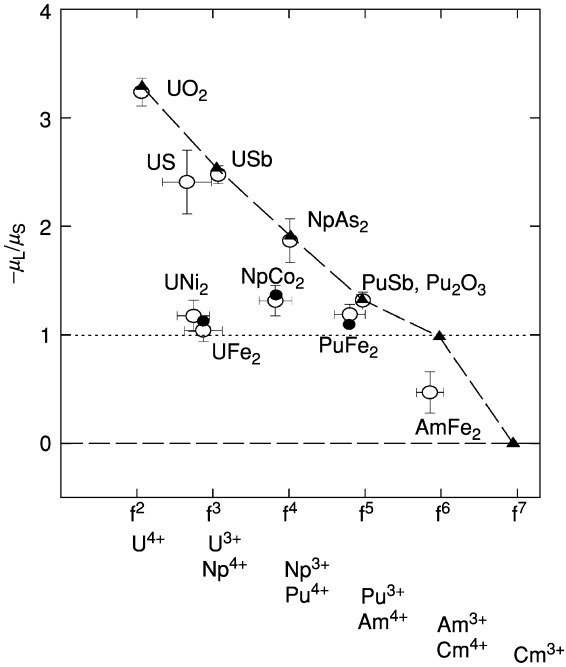

Fig. 21.18 *Ratio of the orbital μ_L and spin μ_S moments in a number of magnetically ordered materials plotted as a function of the number of the 5f-electrons. The triangles, which are connected by a dashed line, are the values derived from single-ion theory including intermediate coupling. Experimental results are shown by open circles. Results of band structure calculations are shown by solid circles.* (*Reprinted from Sechovsky and Havela,* 1998, *with permission from Elsevier.*)

of the same size. Such a case, where the total moment is close to zero, but the spatial extent of spin and orbital moment densities is different, was observed for example in UNi_2 or UFe_2. In the latter case, the U-moment consists of the orbital part $\mu_L = 0.23\mu_B$ and $\mu_S = -0.22\mu_B$. Recently, orbital moments became accessible also in X-ray scattering studies using synchrotron radiation. The strong spin–orbit interaction leads to a characteristic shape for the 5f band consisting of two features, the lower states classified as $j = 5/2$ (containing six states per atom), and the upper states classified as $j = 7/2$ (with eight states per atom). The magnitude of the splitting (up to 3 eV) leads to the formation of a minimum between these features. The weaker tendency to magnetic ordering in Pu systems comparing to Np can be understood as due to the lower sub-band being nearly filled.

A different sensitivity of the spin or orbital moments to external variables led to the assumption that the ratio of orbital and spin moments should reflect the degree of the 5f-delocalization. Indeed, as seen from Fig. 21.18, the compounds showing the least delocalized nature of the 5f states (UO_2, USb, $NpAs_2$, PuSb)

are located on the line representing values of $-\mu_L/\mu_S$ of a free $5f^n$ ion. On the other hand, magnetically ordered materials with presumably the most itinerant 5f states (UFe_2, UNi_2, $NpCo_2$, $PuFe_2$) have this ratio close to 1 (Lander *et al.*, 1991).

Relatively large orbital moments induced by the magnetic field exist probably even in weakly paramagnetic materials like U metal. Surprisingly, in an external magnetic field, the spin and orbital magnetic moments orient parallel to each other, as shown by a simple balance of the Zeeman and spin–orbit energy in the case of weak susceptibility (Hjelm *et al.*, 1993).

21.9.6 Exchange interactions and magnetic anisotropy

Exchange interactions in materials with localized 5f states can be seen as analogous to the lanthanides, for which the indirect exchange of the RKKY-type (oscillatory) is a good approximation. The other limit, systems with strongly itinerant 5f states can be understood in terms of the Stoner–Edwards–Wohlfarth theory for itinerant magnets (one band model), in which the ordering temperature is proportional to the ordered moment. For intermediate delocalization, when the direct 5f–5f overlap is negligible, two types of states have to be considered. 5f states are dominant for the moment formation, but their interaction is mediated by the hybridization with broadband states. Thus a dual role of the 5f–ligand hybridization has to be considered. It destabilizes the 5f magnetic moments, but because the spin information is conserved in the hybridization process, it leads to an indirect exchange coupling. The maximum ordering temperatures consequently can be expected for a moderate strength of hybridization, because a strong hybridization completely suppresses magnetic moments, whereas a weak one leaves moments intact, but their coupling is weak. Cooper and coworkers, on the basis of the Coqblin–Schrieffer approach, have given a model leading to realistic results (Cooper *et al.*, 1985). The mixing term in the Hamiltonian of the Anderson-type is treated as a perturbation, and the hybridization interaction is replaced by an effective f-electron–band-electron resonant exchange scattering. If the ion–ion interaction is considered to be mediated by different covalent-bonding channels, each for a particular magnetic quantum number m_l, then the strongest interaction is for those orbitals, which point along the ion–ion bonding axis, and which represents the quantization axis of the system. The two 5f ions maximize their interaction by compression of the 5f charge towards the direction of the nearest 5f ion. This has serious impacts on magnetic anisotropy, because it means a population of the 5f states with orbital moments perpendicular to the bonding axis. This interaction results in a strong ferromagnetic coupling of actinide atoms along the bonding direction. There is no special general tendency to ferro- or antiferromagnetism in the perpendicular direction, where the interaction is much weaker, and can be comparable to the 'background' isotropic exchange interaction of the standard RKKY-type. Unlike such two-ion hybridization-mediated anisotropy, crystal field (single-ion) effects control the type

and strength of magnetic anisotropy for materials with the localized 5f states, in analogy to lanthanide systems.

The two-ion anisotropy, for which orbital moments are a necessary prerequisite, has been observed in numerous U compounds especially when single-crystal magnetization data exist. The tendency for moments to orient perpendicular to the U—U bonding links leads to a uniaxial anisotropy in crystal structures with U atoms organized in planes with a short in-plane U–U spacing and larger inter-plane spacing, whereas the case of U linear chains leads to a planar type of anisotropy (see Fig. 21.19). The strength of anisotropy, which is observable both in magnetically ordered and paramagnetic phases, can be estimated in some cases from the difference between paramagnetic Curie temperatures when the susceptibility is measured with the magnetic field along different crystallographic directions. Other estimates can be obtained from the extrapolated magnetic field at which magnetization curves along different directions would intersect each other. Typically values of 10^2–10^3 K or 10^2–10^3 Tesla (assuming the anisotropy is energy expressed in k_BT and μ_BH, respectively, where k_B is the Boltzmann constant and μ_B the Bohr magneton) are obtained in this way; see Figs. 21.20 and 21.21).

For large groups of isostructural compounds, the same type of anisotropy is, as a rule, found irrespective of the non-actinide components. The strong generally uniaxial anisotropy of compounds UTX (with the hexagonal structure of the ZrNiAl-type) or tetragonal UT_2X_2, both with strong U bonding within

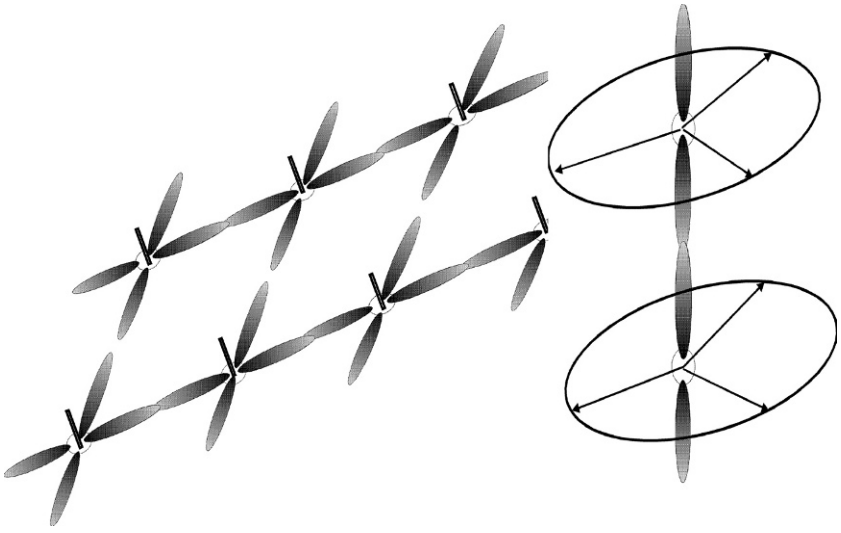

Fig. 21.19 *Schematic view illustrating how the bonding and easy-magnetization directions are related in light actinides. Left part shows the easy-axis anisotropy for planar bonding, right part the easy-plane anisotropy for columnar bonding.* (*Reprinted from Sechovsky and Havela,* 1998, *with permission from Elsevier.*)

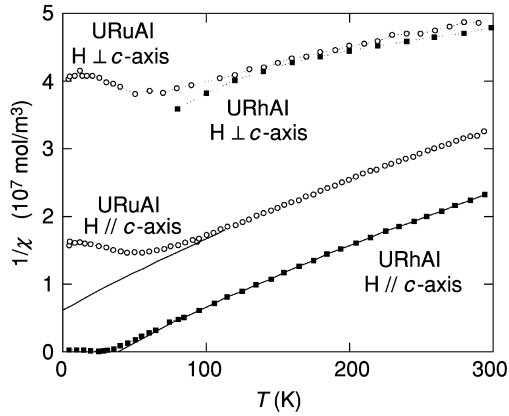

Fig. 21.20 *Temperature dependence of inverse magnetic susceptibility for URuAl and URhAl.* (*Reprinted from Sechovsky and Havela,* 1998, *with permission from Elsevier.*)

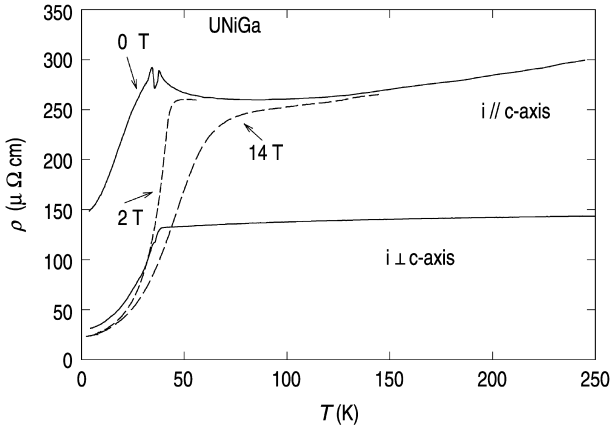

Fig. 21.21 *Temperature dependence of electrical resistivity measured on a single-crystal UNiGa for two current directions and several magnetic field applied along the* c-*axis.* (*Reprinted from Sechovsky and Havela,* 1998, *with permission from Elsevier.*)

planes perpendicular to the hexagonal (tetragonal) axis, and U-moments (or higher susceptibility) along this axis are examples (Sechovsky and Havela, 1998).

21.9.7 Magnetic structures

The specific mechanisms of magnetic anisotropy and exchange interactions both affect the types of magnetic structures in light-actinide materials. Strong anisotropy leads frequently to collinear modulated structures (spin-density

waves), which are preferred over non-collinear equal-moment structures. The reason is that the anisotropy energy is typically stronger than the exchange coupling energies. Non-collinear magnetic structures are stable if the easy-magnetization directions on different sites are non-collinear, as in U_2Pd_2Sn, where they are orthogonal. Also for those cases in which the lattice symmetry imposes no special requirements on the directions of the moments (see Sandratskii, 1998) do non-collinear equal-moment structures appear (e.g. UPtGe). The types of magnetic structures are also affected by the strong ferromagnetic coupling along strong bonding directions (see the hybridization-induced exchange model in Section 21.9.6). For example, the UTX compounds with the hexagonal structure of the ZrNiAl-type tend to magnetic structures consisting of ferromagnetic basal-plane sheets, whereas the inter-sheet exchange interaction is weaker and can be of the ferromagnetic or antiferromagnetic type, leading to a variety of stacking sequences along the hexagonal axis. In this case, ferromagnetic-like alignment can be obtained in moderate magnetic fields applied along the antiferromagnetic stacking direction.

21.9.8 Relation of electronic transport and magnetism – giant magnetoresistance phenomena

The situation in which magnetic moments are strongly coupled to the crystal lattice due to the strong spin–orbit coupling and large orbital moments, and the 5f states are strongly hybridized with other conduction-electron states, is especially favorable to observe any variations of magnetism projected onto electrical resistivity and other transport properties.

The frequently observed anisotropy of exchange coupling (see subsection 21.9.7) often leads to a striking anisotropy in the resistivity. In single crystals of tetragonal, hexagonal, or orthorhombic materials not only the magnitude of resistivity is dependent on the direction of electrical current, but often different directions yield different types of temperature-dependent behavior. In certain directions, antiferromagnetic correlations can be broken by an external magnetic field and a giant magnetoresistance effect can be observed at the critical field. The residual resistivity ρ_0 typically reaches smaller values in ferromagnets. The much larger ρ_0 values observed in antiferromagnets can be understood as due to a gapping of part of the Fermi surface due to an additional periodicity. If, for example, the magnetic structure consists of two sublattices with antiparallel sublattice magnetization, the magnetic unit cell is doubled compared to the crystallographic unit cell (assuming a simple case with one actinide atom in the unit cell). The size of the Brillouin zone is therefore reduced by a factor of 2. As quantum states of electrons must have a gap at every Brillouin zone boundary, a gapping of the Fermi surface will occur if it is cut by the new, inserted, Brillouin zone boundary. This does not bring an extra scattering mechanism, but the effective number of electrons available for the charge transport is reduced, and resistivity therefore increases. This effect is parametrized by the expression:

$$\rho = (\rho_0 + \rho_{\mathrm{e-ph}} + \rho_{\mathrm{e-e}} \ldots)/[1 - g\, m(T)], \tag{21.18}$$

where $m(T)$ is the temperature dependence of sublattice magnetization and g is a truncation factor modifying the Fermi surface. ρ_0, $\rho_{\mathrm{e-ph}}$, $\rho_{\mathrm{e-e}}$ represent individual resistivity terms due to impurity, electron–phonon, and electron–electron scattering, respectively.

The situation can be illustrated by the example of UNiGa (see Fig.21.21), which has an antiferromagnetic ground state. It crystallizes in a layered hexagonal structure (ZrNiAl-type), in which U–Ni and Ni–Al layers alternate along the *c*-axis. Strong ferromagnetic exchange is found within the U–Ni basal planes, where the U-atoms are close together. Magnetic moments are locked along the *c*-axis. The exchange along *c* is weak and antiferromagnetic, and ferromagnetic alignment can be achieved by a magnetic field below 1 T if applied along *c*. The resistivity for current along the *ab*-plane has the character of a ferromagnet, as mostly electrons with the wave vector along *ab* contribute to the conduction. Residual resistivity is low. For current along *c* electrons respond to the antiferromagnetic coupling, and the resistivity is very high. The magnetic unit cell is six times larger than the crystallographic cell along *c*, because the stacking of layers can be described as (++—+–). Fig. 21.21 shows how the high resistivity is suppressed in the metamagnetic state in UNiGa. ρ_0 drops by about 90%. The minimum in $\rho(T)$ for $i//c$ is due to antiferromagnetic correlations above T_{N}, which can be suppressed by the magnetic field (Sechovsky and Havela, 1998).

21.10 COHESION PROPERTIES – INFLUENCE OF HIGH PRESSURE

The variable nature of the 5f electronic states in actinide metals is reflected in cohesion properties. Crystal structures of elemental actinide metals are complex and of low symmetry for the earlier actinides (up to Pu), and they show also relatively higher bulk moduli and few (if any) phase transitions under pressure. In contrast, the transplutonium metals do not have the 5f electrons involved in bonding, their atomic volumes are much higher, and they are softer, i.e. with lower bulk moduli. Application of pressure induces a sequence of structural phase transitions, eventually reaching states with itinerant 5f states with corresponding low atomic volumes and low-symmetry structures. In Fig. 21.22, the phase diagram for Ac through Cf as a function of pressure is shown from a more detailed discussion by Lindbaum *et al.* (2003). The reason why the 5f bonding leads to smaller atomic volumes can be seen from two points of view. One is the smaller spatial extent of the 5f states even in bonding situations, when compared to the other bonding states (6d, 7s), as described in section 21.4.1. The bonding energy minimum evaluated for the separate 5f states appears at much smaller inter-atomic spacing than for the 6d–7s states. The real equilibrium volume, obtained by summing both contributions, corresponds

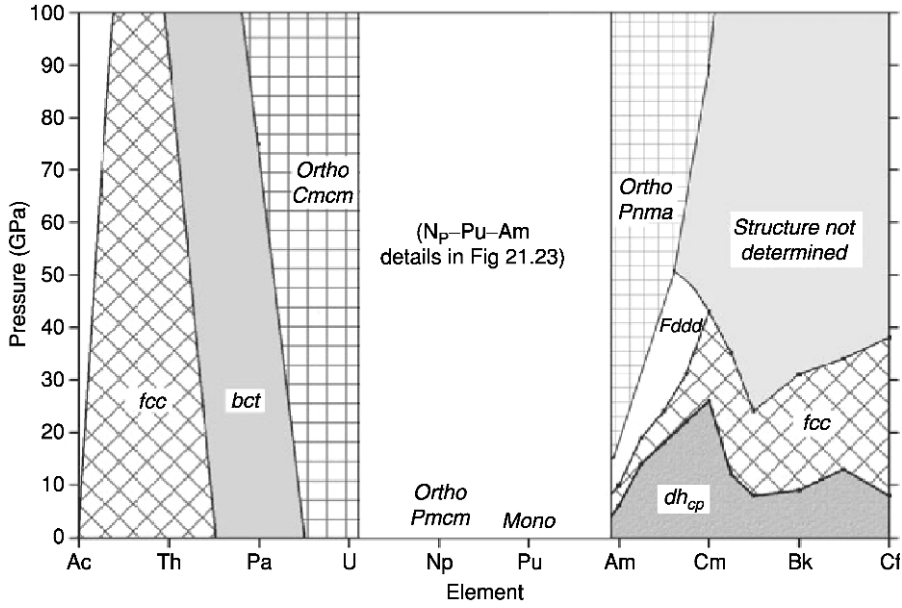

Fig. 21.22 *Phase diagram of the actinides* (*Ac through Cf*) *vs pressure. The complexity of the pressure phase diagram depends in large part on the role of the 5f electrons in bonding and variations in bonding as the interatomic distances are decreased under pressure* (*after Lindbaum* et al., 2003).

then to a compromise between the smaller 5f and larger 6d–7s bonding distance. Releasing the 5f states from bonding leads to the 6d–7s bonding only, with its larger bonding length. The second reason for the volume expansion is the different screening of the ionic potential, attracting the outer (6d–7s) electrons to the ion core. When withdrawn from bonding, the 5f charge density redistributes more towards the ion core, which screens more effectively the attractive potential, and the less attracted 6d and 7s states expand.

The existence of the low-symmetry structures for itinerant 5f electronic states can be caused by an electronic Jahn–Teller effect. In this situation, when the density of electronic states in the vicinity of the Fermi level reaches appreciable values, the total energy can be minimized by redistributing some of the 5f band states towards lower energies, using the degrees of freedom offered by all possible exotic crystal structures. For these high densities of states, such distortions can compensate the loss of the Madelung energy, which favors high-symmetry structures. One can compare this situation with e.g. the late 3d transition metals, similarly characterized by high $N(E_F)$ values. In such a case, the Stoner criterion $U.N(E_F) > 1$ is fulfilled, which leads to magnetic order. Thus the ground state for high $N(E_F)$ values can be either magnetic (in case of sufficient high U) or a low-symmetry crystal structure, if U is not large enough.

The latter case holds in the early actinide metals and in the late actinides in the high-pressure phases. An interesting insight is provided by *ab initio* electronic structure calculations in different structure types (see for example, Wills and Eriksson, 1992 or 2000).

Although specialized review chapters exist covering the structural aspects of actinides at high pressures (Benedict, 1987; Benedict and Holzapfel, 1993), the enormous progress in the last decade has brought numerous new data (extended pressure ranges led to discovery of new phases, improved hydrostatic conditions yield much more precise values of bulk moduli), so that it is worthwhile to provide a more detailed overview for the individual metals. Thorium crystallizes in the fcc structure, but at very high pressure (between 75 and 100 GPa), it undergoes a transition to a body-centered tetragonal structure (Vohra and Akella, 1991). Calculations show that the high-pressure structure can be associated with a population of the 5f band of about 0.6 electrons (Rao *et al.*, 1992). This structure is the same as adopted by protactinium at ambient pressure. Pa bulk modulus value, 118(2) GPa obtained from a recent experiment (Le Bihan *et al.*, 2003), is much closer to the value of 100 GPa predicted by calculations (Söderlind and Eriksson, 1997) than previous data (Benedict *et al.*, 1982). The new experiment also revealed a structural phase transition at 77(5) GPa identified as the α-U structure (Haire *et al.*, 2003). The reason for this structure change can be seen in somewhat varying (increasing) 5f occupancy at lower volume.

The same argument, i.e. higher 5f occupancy, is why the orthorhombic α-U structure (*Cmcm* space group) stabilizes in uranium. Its bulk modulus 104(2) GPa (Le Bihan *et al.*, 2003) is similar to the value for Pa. Some authors, though, give higher values. For a review of older data, see Benedict (1987) and Benedict and Holzapfel (1993). The α-U structure is stable to at least 100 GPa, in agreement with theory (Le Bihan *et al.*, 2003). The ground state structure of neptunium (orthorhombic, space group *Pmcn*) was found to be similarly stable to at least 52 GPa (Dabos *et al.*, 1987). The bulk modulus of 118(2) GPa is comparable with the value of 110 GPa obtained from calculations (Johansson and Skriver, 1982).

The qualitative difference of cohesion properties in transplutonium materials is well illustrated by the case of americium (Heathman *et al.*, 2000; Lindbaum *et al.*, 2001). The initial bulk modulus of 30 GPa leads to a rapid decrease of the volume with applied pressure. A sequence of structural phase transitions starts at 6.1 GPa, at which pressure the dhcp ground-state structure (the same as for Cm, Bf, and Cf) transforms into a fcc structure. The next transition at 11 GPa, accompanied by a volume collapse of 2%, leads to an orthorhombic structure, which is identical with the γ-Pu structure. It has been proposed that this structure already shows 5f bonding. An even larger volume collapse of 7% appears at 16 GPa, and brings Am into an orthorhombic structure with a low compressibility, similar to the α-U-type, and thus confirming the itinerant nature of the 5f states. The volume collapse and 5f bonding was predicted also by theory, although one type of calculation preferred the α-Pu structure as the high-pressure phase (Söderlind *et al.*, 2000). On the other hand, calculations of

Pénicaud (2002) are not only consistent with the real orthorhombic structure, but suggest that this so-called Am(IV) structure is also one of the high-pressure structures of Pu. Although Pu has been studied thoroughly, information is lacking in the open literature for the high-pressure range, clearly due to nuclear non-proliferation concerns. But the data available confirm the stability of the α-Pu phase up to 40 GPa (Benedict and Holzapfel, 1993 and Dabos-Seignon *et al.*, 1993). On the other hand, the expanded-volume δ-phase collapses again under a pressure of several few kbar (1 kbar = 0.1 GPa). The opposite experiment, i.e. imposing a negative pressure by doping larger Am atoms, shows that the δ-Pu phase is stabilized over a large concentration range and corresponds actually to the Am(II) fcc structure. Recent results for Cm indicate a lattice structure stabilized by magnetism (Heathman *et al.*, 2005). The interplay between pressure and alloy substitution is shown very nicely in Fig. 21.23 for the Np, Pu, Am solid solution series. The inset in the upper left corner of Fig. 21.23 shows elemental Pu as a function of pressure. There is a strong resemblance to the phases obtained from alloys of Pu with Np, which effectively increases the pressure in the Pu lattice (Hecker, 2000).

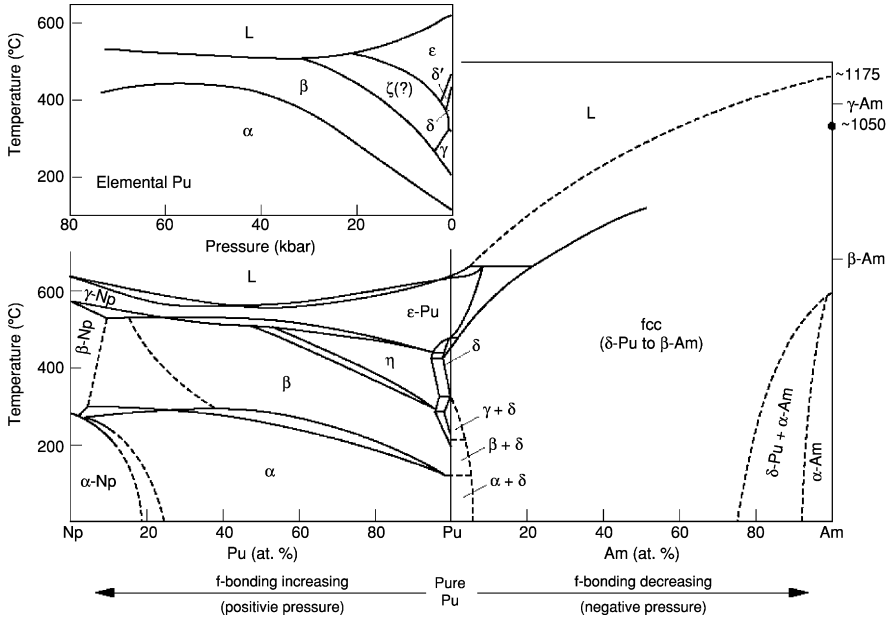

Fig. 21.23 *The binary phase diagram for Np through Am as a function of temperature. The inset in the upper left shows the temperature vs pressure phase diagram for Pu metal. The similarity between the Pu pressure diagram and the Np–Pu binary gives clear indication of how atomic substitution may create effective pressure in metallic solids* (*after Hecker,* 2000).

21.11 CONCLUDING REMARKS

There remains a great deal of uncertainty regarding the understanding of the actinides in the metallic state. For the late actinide metals, much of the uncertainty arises from sample size and purity limitations. For the early actinides (through Pu), the uncertainty is centered on the understanding of the 5f electrons and the nature of the narrow bands in actinide metals. The literature presents many models for treating the 5f electrons from Th through Pu with no clear consensus model for the electronic structure, which is universally applicable. In many cases, it appears that the 5f electrons form narrow bands, which hybridize with the conduction electrons to some extent and give rise to many of the interesting properties of actinides in the metallic state. By expanding the phase space of investigation to include alloys, compounds, and pressure one finds some systematics in the properties of actinide metals. Indeed, Fig. 21.23 demonstrates how pressure and alloying may be considered equivalent knobs to adjust in tuning the properties of metallic actinides. The propensity for rich electronic structure in the metallic actinides is highlighted by the frequent occurrence of correlated electron ground states including magnetism (both local moment and band magnetism), enhanced mass, superconductivity, and charge-density waves. The rich electronic structure is indicative of nearly degenerate energy scales and competing processes to lower the free energy. In the most complex systems, one finds competing ordered ground states such as enhanced mass and superconductivity in UPt_3 and UBe_{13} with truly exceptional characteristics in materials like UPd_2Al_3, which exhibits enhanced mass, magnetism, and superconductivity. The discovery of superconductivity at 18 K in $PuCoGa_5$ in 2002 (Sarrao *et al.*, 2002) ushers in a new era for actinide superconductivity spanning the gap between low-temperature spin-fluctuators and the high temperature oxides exhibiting charge fluctuations. While an uncontested explanation for the electronic properties of metallic actinides is still in the future, the broader understanding of actinide alloys and compounds, along with increased range in pressure and temperature phase space, gives us a better understanding of the intricacies of the elemental actinides in the metallic state such as the charge-density waves in uranium metal as well as the multiple phases, crystal structures, and volumes of plutonium metal.

ABBREVIATIONS

Å	Angström
AF	anti-ferromagnetic
An	actinide
ARPES	angle resolved photoemission
bcc	body-centered cubic
bct	body-centered-tetragonal

T_c	critical temperature
T_C	Curie temperature
DFT	density functional theory
dhcp	double hexagonal close-packed
dHvA	de Haas–van Alpen
DOS	density of states
DMFT	Dynamical Mean Field Theory
m^*	Effective mass
fcc	face-centered cubic
E_F	Fermi Energy
FL	Fermi Liquid
FM	Ferromagnetic
γ	low temperature specific heat coefficient
GGA	generalized gradient approximation
hcp	hexagonal close-packed
LDA	local density approximation
χ	magnetic susceptibility
mono	monoclinic
T_N	Néel temperature
NFL	Non-Fermi-Liquid
orth	Orthorhombic
PAM	Periodic Anderson Model
PES	photoelectron spectroscopy
RKKY	Ruderman-Kittel-Kasuya-Yosida
SC	Superconducting
SIM	single impurity model

ACKNOWLEDGMENTS

Thanks to James L. Smith for a great deal of assistance in figures and scientific input, and in general to John Wills, Jim Smith, Olle Eriksson, and Mike Boring for discussions and previous work which J.J. and A.A. relied heavily upon in writing this review. This work was supported by the U.S. Department of Energy, Office of Science. The work of L.H. at the Charles University was part of the research program MSM 002160834 financed by the Ministry of Education of the Czech Republic.

REFERENCES

Aeppli, G., Bucher, E., Broholm, C., Kjems, J. K., Baumann, J., and Hufnagl, J. (1988) *Phys. Rev. Lett.*, **60**, 615.

Aldred, A. T., Cinader, G., Lam, D. J., and Weber, L. W. (1979) *Phys. Rev. B,* **19**, 300–5.

Andreev, A. V., Belov, K. P., Deriagin, A. V., Levitin, R. Z., and Menovsky, A. (1979) *J. Phys. (Paris),* **40**, C4, 82–3.

Andres, K., Davidov, D., Dernier, P., Hsu, F., and Reed, W. A. (1978) *Solid State Commun.,* **28**, 405–8.

Arko, A. J., Brodsky, M. B., and Nellis, W. J. (1972) *Phys. Rev. B,* **5**, 4564.

Arko, A. J., Fradin, F. Y., and Brodsky, M. B. (1973) *Phys. Rev. B,* **8**, 4104.

Arko, A. J., Koelling, D. D., and Reihl, B. (1983) *Phys. Rev. B,* **27**, 3955.

Arko, A. J., Koelling, D. D., and Schirber, J. E. (1985) Energy band structure and fermi surface of actinide materials, in *Handbook on the Physics and Chemistry of the Actinides,* vol. 1 (eds. A. J. Freeman and G. H. Lander), Elsevier, Amsterdam, pp. 175–238.

Arko, A. J., Andrews, A. B., Riseborough, P. S., Joyce, J. J., Tahvildar-Zadeh, A., and Jarrell, M. A. (1999) Photoelectron spectroscopy in heavy fermion systems: emphasis on single crystals, in *Handbook on the Physics and Chemistry of Rare Earths*, vol. 26, Elsevier Science, Amsterdam, p. 265, ch. 172.

Ashcroft, N. E. and Mermin, N. D. (1976) *Solid State Physics,* Holt, Rinhart and Winston, Philadelphia.

Bader, S. D., Phillips, N. E., and Fisher, E. S. (1975) *Phys. Rev. B,* **12**, 4929–40.

Baer, Y. (1984) Electron spectroscopy studies, in *Handbook on the Physics and Chemistry of the Actinides,* vol. 1 (eds. A. J. Freeman and G. H. Lander), Elsevier, Amsterdam, p. 271.

Ballou, R. (1983) Thesis, University of Grenoble.

Bardeen, J., Cooper, L. N., and Schrieffer, J. R. (1957) *Phys. Rev.,* **108**, 1175.

Bauer, E. D., Thompson, J. D., Sarrao, J. L., Morales, L. A., Wastin, F., Rebizant, J., Griveau, J. C., Javorsky, P., Boulet, P., Colineu, E., Lander, G. H., and Stewart, G. R. (2004) *Phys. Rev. Lett.,* **93**, 147005.

Benedict, U., Spirlet, J. C., Dufour, C., Birkel, I., Holzapfel, W. B., and Peterson, J. R. (1982) *J. Magn. Magn. Mater.,* **29**, 287–90.

Benedict, U. (1987) The effect of high pressures on actinide metals, in *Handbook on the Physics and Chemistry of the Actinides,* vol. 5 (eds. A. J. Freeman and G. H. Lander), Elsevier, Amsterdam, pp. 227–69.

Benedict, U. and Holzapfel, W. B. (1993) High-pressure studies – structural aspects, in *Handbook on the Physics and Chemistry of Rare Earths,* vol. 17 (eds. K. A. Gschneidner Jr, L. Eyring, G. H. Lander, and G. Choppin), Elsevier, Amsterdam, pp. 245–300, ch. 113.

Berlureau, T., Chevalier, B., Gravereau, P., Fournès, L., and Etourneau, J. (1991) *J. Magn. Magn. Mater.,* **102**, 166–74.

Bernhoeft, N., Sato, N., Roessli, B., Aso, N., Hiess, A., Lander, G. H., Endoh, Y., and Komatsubara, T. (1998) *Phys. Rev. Lett.,* **81**, 4244.

Bernhoeft, N., Lander, G. H., Longfield, M. J., Langridge, S., Mannix, D., Lidström, E., Colineau, E., Hiess, A., Vettier, C., Wastin, F., Rebizant, J., and Lejay, P. (2003) *Acta Phys. Pol. B,* **23**, 1367.

Bloch, F. (1928) *Z. Phys.,* **52**, 555.

Boring, A. M. and Smith, J. L. (2000) *Los Alamos Science*, vol. 26 (ed. N.G. Cooper), Los Alamos National Laboratory.

Buschow, K. H. J. (1971) *J. Appl. Phys.,* **42**, 3433.

Buyers, W. J. L. and Holden, T. (1985) Neutron scattering from spins and phonons in actinide systems, in *Handbook on the Physics and Chemistry of the Actinides,* vol. 2, (eds. A. J. Freeman and G. H. Lander), Elsevier, Amsterdam, pp. 239–327.

Chandra, P., Coleman, P., Mydosh, J. A., and Tripathi, V. (2002) *Nature,* **417**, 831.

Chen, J. W., Hake, R. R., Lambert, S. E., Maple, M. B., Rossel, C., Torikachvili, M. S., and Yang, K. N. (1985) *J. Appl. Phys.,* **57**, 3090.

Cooper, B. R., Siemann, R., Yang, D., Thayamballi, P., and Banerjea, A. (1985) Hybridization induced anisotropy in cerium and actinide systems, in *Handbook on the Physics and Chemistry of the Actinides,* vol. 2 (eds. A. J. Freeman and G. H. Lander), Elsevier, Amsterdam, pp. 435–98.

Dabos, S., Dufour, C., Benedict, U., and Pages, M. (1987) *J. Magn. Magn. Mater.,* **63 & 64**, 661–3.

Dabos-Seignon, S., Dancausse, J. P., Gering, E., Heathman, S., and Benedict, U. (1993) *J. Alloys and Compd.,* **190**, 237–42.

Deryagin, A. V. and Andreev, A. V. (1978) *Sov. Phys. JETP,* **44**, 610–13.

Dreitzler, R. M. and Gross, E. K. U. (1990) *Density Functional Theory,* Springer-Verlag, Berlin.

Dunlap, B. D. and Kalvius, G. M. (1985) Mössbauer spectroscopy on actinides and their compounds, in *Handbook on the Physics and Chemistry of the Actinides,* vol. 2 (eds. A. J. Freeman and G. H. Lander), Elsevier, Amsterdam, pp. 329–434.

Eriksson, O., Johansson, B., Brooks, M. S. S., and Skriver, H. L. (1989) *Phys. Rev. B,* **40**, 9519.

Eriksson, O., Becker, J. D., Balatsky, A. V., and Wills, J. M. (1999) *J. Alloys compd.,* **287**, 1–5.

Fano, U. (1961) *Phys. Rev.,* **124**, 1866.

Fisk, Z., Ott, H. R., and Smith, J. L. (1985) *Physica,* **130B**, 159–62.

Flouquet, J., Huxley, A., Braithwaite, D., Hardy, F., Knebel, G., Mineev, V., Ressouche, E., Aoki, D., and Brison, J. P. (2003) *Acta Phys. Pol. B,* **34**, 275.

Fournier, J. M. and Troc, R. (1985) Bulk properties of the actinides, in *Handbook on the Physics and Chemistry of the Actinides,* vol. 2 (eds. A. J. Freeman and G. H. Lander), North-Holland, Amsterdam, pp. 29–179.

Fournier, J. M., Boeuf, A., Frings, P., Bonnet, M., Boucherle, J. X., Delapalme, A., and Menovsky, A. (1986) *J. Less Common Metals,* **121**, 249–52.

Fournier, J. M. and Gratz, E. (1993) in *Handbook on the Physics and Chemistry of Rare Earths,* vol. 17 (eds. K. A. Gschneidner Jr, L. Eyring, G. H. Lander, G. R. Choppin), North-Holland, Amsterdam, pp. 409–537.

Fowler, R. D., Matthias, B. T., Asprey, L. B., Hill, H. H., Lindsay, J. D. G., Olsen, C. E., and White, R. W. (1965) *Phys. Rev. Lett.,* **15**, 860.

Franse, J. J. M., Frings, P. H., de Boer, F. R., and Menovsky, A. (1981) in *Physics of Solids under High Pressure* (eds. J. S. Schilling and R. N. Shelton), North-Holland, Amsterdam, p.181.

Franse, J. J. M., Frings, P. H., de Visser, A., Menovsky, A., Palstra, T. T. M., and Mydosh, J. A. (1984) *Physica B,* **126**, 116.

Friedel, J. (1969) *The Physics of Metals* (ed. J. M. Ziman), Cambridge University Press, New York.

Geibel, C., Thies, S., Kaczorowski, D., Mehner, A., Garuel, A., Seidel, B., Ahlheim, U., Helfrich, R., Petersen, K., Bredl, C. D., and Steglich, F. (1991) *Z. Phys. B,* **83**, 305.

Gordon, P. (1949) Thesis, Massachusetts Institute of Technology.

Gordon, J. E., Montgomery, H., Noer, R. J., Pickett, G. R., and Tobón, R. (1966) *Phys. Rev.,* **152**, 432.

Gouder, T., Wastin, F., Rebizant, J., and Havela, L. (2000) *Phys. Rev. Lett.,* **84**, 3378.

Gouder, T., Havela, L., Divis, M., Rebizant, J., Oppeneer, P. M., and Richter, M. (2001) *J. Alloys Compd.,* **314**, 7–14.

Greiner, J. D. and Smith, J. F. (1971) *Phys. Rev. B,* **4**, 3275.

Grewe, N. and Steglich, F. (1991) in *Handbook on the Physics and Chemistry of Rare Earths,* vol. 14 (eds. K. A. Gschneidner Jr and L. Eyring), North-Holland, Amsterdam, p. 343.

Griveau, J.-C., Pfleiderer, C., Boulet, P., Rebizant, J., and Wastin, F. (2004) *J. Magn. Magn. Mater.,* **272–276**, 154.

Gschneidner, K. A. Jr and Eyring, L. (eds.) (1993) *Handbook on the Physics and Chemistry of Rare Earths,* vol. 17, , North-Holland, Amsterdam.

Haire, R. G., Heathman, S., Iridi, M., Le Bihan, T., Lindbaum, A., and Rebizant, J. (2003) *Phys. Rev. B,* **67**, 134101.

Harrison, W. A. (1980) *Solid State Theory,* Dover, New York.

Harrison, W. A. (1999) *Elementary Electronic Structure,* World Scientific, Singapore.

Havela, L., Gouder, T., Wastin, F., and Rebizant, J. (2002) *Phys. Rev. B,* **65**, 235118.

Havela, L., Wastin, F., Rebizant, J., and Gouder, T. (2003) *Phys. Rev. B,* **68**, 085101.

Heathman, S., Haire, R. G., Le Bihan, T., Lindbaum, A., Litfin, K., Mèresse, Y., and Libotte, H. (2000) *Phys. Rev. Lett*. **85**, 2961.

Heathman, S., Haire, R. G., Le Bihan, T., Lindbaum, A., Idira, M., Normile, P., Li, S., Ahuja, R., Johansson, B., and Lander, G. H., (2005) *Science* **309**, 110.

Hecker, S. S. (2000) *Los Alamos Science*, vol. 26 (ed. N.G. Cooper).

Hecker, S. S. (2001) *MRS Bull.,* **26** (9), 672.

Hecker, S. S., Harbur, D. R., and Zocco, T. G. (2004) *Prog. Mater. Sci.,* **49**, 429.

Heffner, R. J., Smith, J. L., Willis, J. O., Birrer, P., Baines, C., Gygax, F. N., Hitti, B., Lippelt, E., Ott, H. R., Schenk, A., Knetsch, E. A., Mydosh, J. A., and McLaughlin, D. E. (1990) *Phys. Rev. Lett.,* **65**, 2816.

Hein, R. A., Henry, W. E., and Wolcott, N. M. (1957) *Phys. Rev.,* **107**, 1517.

Hill, H. H. (1970) in: *Plutonium and Other Actinides,* ed. W. N. Miner (AIME, New York) p.2.

Hjelm, A., Eriksson, O., and Johansson, B. (1993) *Phys. Rev. Lett.,* **71**, 1459–61.

Hohenberg, P. and Kohn, W. (1964) *Phys. Rev. B,* **136**, 864.

Holland-Moritz, E. and Lander, G. H. (1994) in *Handbook on the Physics and Chemistry of Rare Earths,* vol. 19. (eds. K. A. Gschneidner Jr, L. Eyring, G. H. Lander, and G. R. Choppin), North-Holland, Amsterdam, pp. 1–120.

Huray, P. G. and Nave, S. E. (1987) in *Handbook on the Physics and Chemistry of the Actinides,* vol. 5. (eds. A. J. Freeman and S. E. Nave), Elsevier, Amsterdam.

Johansson, B. and Skriver, H. L. (1982) *J. Magn. Magn. Mater.,* **29**, 217.

Johansson, B. and Brooks, M. S. S. (1993) in *Handbook on the Physics and Chemistry of Rare Earths,* vol. 17 (eds. K. A. Gschneidner Jr, L. Eyring, G. H. Lander, and G. R. Choppin), North-Holland, Amsterdam, pp. 149–244.

Joyce, J. J., Arko, A. J., Cox, L., and Czuchlewski, S. (1998) *Surf. Interface Anal.,* **26**, 121.

Joyce, J. J., Wills, J. M., Durakiewicz, T., Butterfield, M. T., Guziewicz, E., Sarrao, J. L., Morales, L. A., Arko, A. J., and Eriksson, O. (2003) *Phys. Rev. Lett.,* **91**, 176401.

Joyce, J. J., Wills, J. M., Durakiewicz, T., Guziewicz, E., Butterfield, M. T., Arko, A. J., Moore, D. P., Sarrao, J. L., Morales, L. A., and Eriksson, O. (2004) *Mat. Res. Soc. Symp. Proc.,* **802**, 239–44.

Kanellakopulos, B., Blaise, A., Fournier, J. M., and Muller, W. (1975) *Solid State Commun.,* **17**, 713–15.
Kevan, S. D. (ed.) (1992) *Angle-Resolved Photoemission Theory and Current Applications,* Elsevier, Amsterdam.
Kittel, C. (1963) *Quantum Theory of Solids,* John Wiley, New York.
Kittel, C. (1971) *Introduction to Solid State Physics,* John Wiley, New York.
Koelling, D. D., Dunlap, B. D., and Crabtree, G. W. (1985) *Phys. Rev. B,* **31**, 4966–71.
Kohn, W. and Sham, L. J. (1965) *Phys. Rev. A,* **140**, 1133.
Krimmel, A., Fischer, P., Roessli, B., Maletta, H., Geibel, C., Schank, C., Grauel, A., Loidl, A., and Steglich, F. (1993) *Z. Phys. B,* **86**, 161.
Landau, L. (1957) *Sov. Phys. JETP,* **3**, 920.
Lander, G. H., Brooks, M. S. S., and Johansson, B. (1991) *Phys. Rev. B,* **43**, 13672–5.
Lander, G. H., Fisher, E. S., and Bader, S. D. (1994) *Adv. Phys.,* **43**, 1–110.
Lashley, J. C., Singleton, J., Migliori, A., Betts, J. B., Fisher, R. A., Smith, J. L., and McQueeney, R. J. (2003) *Phys. Rev. Lett.,* **91**, 205901.
Le Bihan, T., Heathman, S., Idiri, M., Wills, J. M., Lawson, A. C., and Lindaum, A. (2003) *Phys. Rev. B,* **67**, 134102.
Ledbetter, H. M. and Moment, R. L. (1976) *Acta Metall.,* **24**, 891–9.
Lindbaum, A., Heathman, S., Litfin, K., Méresse, Y., Haire, R.G., Le Bihan, T., and Libotte, H. (2001) *Phys. Rev. B,* **63**, 214101.
Lindbaum, A., Heathman, S., Le Bihan, T., Haire, R. G., Diri, M. I., and Lander, G. H. (2003) *J. Phys.: Condens. Matter,* **15**, S2297.
Louie, S. G. (1992) Quasiparticle excitation and photoemission, in *Angle-Resolved Photoemission Theory and Current Applications* (ed. S. D. Kevan), Elsevier, Amsterdam.
Luttinger, J. M. (1960) *Phys. Rev.,* **119**, 1153.
Maple, M. B., Chen, J. W., Dalichaouch, Y., Kohara, T., Rossel, C., Torikachvili, M. S., McElfresh, M. W., and Thompson, J. D. (1986) *Phys. Rev. Lett.,* **56**, 185.
McEwen, K. A., Steinberger, U., and Martinez, J. L. (1993) *Physica B,* **186–188**, 670–4.
Méot-Reymond, S. and Fournier, J. M. (1996) *J. Alloys Compd.,* **232**, 119–25.
Merrifield, R. E. (1966) *J. Chem. Phys.,* **44**, 4005.
Mortimer, M. J. (1979) *J. Phys.* (*Paris*) (*C-4*), **40**, 124.
Naegele, J. R., Ghijen, J., and Manes, L. (1985) Localization and hybridization of 5f states in the metallic and ionic bond as investigated by photoelectron spectroscopy, in *Actinides – Chemical and Physical Properties* (ed. L. Manes), Structure and Bonding 59/60, Springer-Verlag, Berlin, p. 198.
Nellis, W. J. and Brodsky, M. B. (1974) in *The Actinides: Electronic Structure and Related Properties,* vol. 2. (eds. A. J. Freeman and J. B. J. Darby), Academic Press, New York, pp. 265–88.
Nieuwenhuys, G. J. (1995) in *Handbook of Magnetic Materials,* vol. 9 (ed. K. H. J. Buschow), North-Holland, Amsterdam, pp. 1–55.
Niklasson, A. M. N., Wills, J. M., Katsnelson, M. I., Abrikosov, I. A., Eriksson, O., and Johansson, B. (2003) *Phys. Rev. B,* **67**, 235105.
Norman, M. R. and Koelling, D. D. (1993) in *Handbook on the Physics and Chemistry of Rare Earths,* vol. 17 (eds. K. A. Gschneidner Jr, L. Eyring, G. H. Lander, and G. R. Choppin), North-Holland, Amsterdam, pp. 1–86.
Olsen, C. E., Comstock, A. L., and Sandenaw, T. A. (1992) *J. Nucl. Mater.,* **195**, 312–16.

Ott, H. R., Rudigier, H., Fisk, Z., and Smith, J. L. (1983) *Phys. Rev. Lett.,* **50**, 1595.
Ott, H. R. and Fisk, Z. (1987) Heavy-electron actinide materials, in *Handbook on the Physics and Chemistry of Rare Earths,* vol. 17 (eds. A. J. Freeman and G. H. Lander), North-Holland, Amsterdam, pp. 85–225.
Pénicaud, M. (2002) *J. Phys.: Condens. Matter,* **14**, 3575.
Petit, L., Svane, A., Szotek, Z., and Temmerman, W. M. (2003) *Science,* **301**, 498–501.
Poon, S. J., Drehman, A. J., Wong, K. M., and Clegg, A. W. (1985) *Phys. Rev. B,* **31**, 3100.
Potzel, W., Kalvius, G. M., and Gal, J. (1993) in *Handbook on the Physics and Chemistry of Rare Earths,* vol. 17 (eds. K. A. Gschneidner Jr, L. Eyring, G. H. Lander, and G. R. Choppin), North-Holland, Amsterdam, pp. 539–634.
Rao, R. S., Godwal, B. K., and Sikka, S. K. (1992) *Phys. Rev. B,* **46**, 5780.
Reihl, B., Domke, M., Kaindl, G., Kalkowski, G., Laubschat, C., Hulliger, F., and Schneider, W. D. (1985) *Phys. Rev. B,* **32**, 3530–3.
Rogl, P. (1991) The ternary and higher order systems with actinide elements and boron, in *Handbook on the Physics and Chemistry of the Actinides* (eds. A. J. Freeman and G. Keller), North-Holland, Amsterdam, pp. 75–154.
Sanchez-Castro, C. and Bedell, K. S. (1993) *Phys. Rev. B,* **47**, 1203.
Sandratskii, L. M. (1998) *Adv. Phys.,* **47**, 91–160.
Sarrao, J. L., Morales, L. A., Thompson, J. D., Scott, B. L., Stewart, G. R., Wastin, F., Rebizant, J., Boulet, P., Colineau, E., and Lander, G. H. (2002) *Nature,* **420**, 297.
Sato, N. K., Aso, N., Miyake, K., Shiina, R., Thalmeier, P., Varelogiannis, G., Geibel, C., Steglich, F., Fulde, P., and Komatsubara, T. (2001) *Nature,* **410**, 340–3.
Savrasov, S. Y., Kotliar, G., and Abrahams, E. (2001) *Nature,* **410**, 793.
Saxena, S. S., Agarwal, P., Ahilan, K., Grosche, F. M., Haselwimmer, R. K. W., Steiner, M. J., Pugh, E., Walker, I. R., Julian, S. R., Monthoux, P., Lonzarich, G. G., Huxley, A., Sheikin, I., Brathwaite, D., and Flouquet, J. (2000) *Nature,* **406**, 587.
Sechovský, V. and Havela, L. (1988) in *Ferromagnetic Materials – A Handbook on the Properties of Magnetically ordered Substances,* vol. 4 (eds. E. P. Wohlfarth and K. H. J. Buschow), North-Holland, Amsterdam, pp. 309–491.
Sechovský, V. and Havela, L. (1998) in *Handbook of Magnetic Materials,* vol. 11 (ed. K. H. J. Buschow), North-Holland, Amsterdam, pp. 1–289.
Shick, A. B., Drchal, V., and Havela, L. (2005) *Europhys. Lett.,* **69**, 588–94.
Slater, J. C. (1937) *Phys. Rev.,* **51**, 846.
Smith, J. L. and Haire, R. G. (1978) *Science,* **200**, 535.
Smith, J. L., Stewart, G. R., Huang, C. Y., and Haire, R. G. (1979) *J. Phys.* (*Paris*) (*C-4*), **40**, 138.
Smith, J. L. and Kmetko, E. A. (1983) *J. Less Common Metals,* **90**, 83.
Spirlet, J. C., Hall, R. A. O., Jeffrey, A. J., and Mortimer, M. J. (1987) *Proc 17emes Journees des Actinides* (*Signal des Chexbres*), ed. P. Erdös, p. 15.
Steglich, F., Aarts, J., Bredl, C. D., Lieke, W., Meschede, D., Franz, W., and Schafer, H. (1979) *Phys. Rev. Lett.,* **43**, 1892–6.
Stevenson, J. N. and Peterson, J. R. (1979) *J. Less Common Metals,* **66**, 201–10.
Stewart, G. R., Fisk, Z., Willis, J. O., and Smith, J. L. (1984) *Phys. Rev. Lett.,* **52**, 679.
Stewart, G. R. (2001) *Rev. Mod. Phys.,* **73**, 797.
Söderlind, P., Eriksson, O., Johansson, B., Wills, J. M., and Boring, A. M., (1995) *Nature,* **374**, 524.

Söderlind, P. and Eriksson, O. (1997) *Phys. Rev. B,* **56**, 10719.
Söderlind, P., Ahuja, R., Eriksson, O., Johansson, B., and Wills, J. M. (2000) *Phys. Rev. B,* **61**, 8119.
Söderlind, P. and Sadigh, B. (2004) *Phys. Rev. Lett.,* **92**, 185702.
Vogt, O. and Mattenberger, K. (1993) in *Handbook on the Physics and Chemistry of Rare Earths,* vol. 17 (eds. K. A. Gschneidner Jr, L. Eyring, G. H. Lander, and G. R. Choppin), North-Holland, Amsterdam, pp. 301–407.
Vohra, Y. K. and Akella, J. (1991) *Phys. Rev. Lett.,* **67**, 3563.
Wiesinger, G. and Hilscher, G. (1991) in *Handbook of Magnetic Materials,* vol. 6 (ed. K. H. J. Buschow), Elsevier, Amsterdam.
Wigner, E. P. and Seitz, F. (1933) *Phys. Rev.,* **43**, 804.
Wigner, E. (1934) *Phys. Rev.,* **46**, 1002.
Wills, J. M. and Eriksson, O. (1992) *Phys. Rev. B,* **45**, 13879.
Wills, J. M. and Eriksson, O. (2000) *Los Alamos Science*, vol. 26 (ed. N.G. Cooper), Los Alamos National Laboratory.
Wills, J. M., Eriksson, O., Delin, A., Andersson, P. H., Joyce, J. J., Durakiewicz, T., Butterfield, M. T., Arko, A. J., Moore, D. P., and Morales, L. A. (2004) *J. Electron. Spectrosc. Relat. Phenom.,* **135**, 163–66.
Wong, J., Krisch, M., Farber, D. L., Occelli, F., Schwartz, A. J., Chiang, T. C., Wall, M., Boro, C., and Xu, R. Q. (2003) *Science* **301**, 1078–80.
Zachariasen, W. H. (1973) *J. Inorg. Nucl. Chem.,* **35**, 3487–97.
Ziman, J. M. (1972) *Principles of the Theory of Solids,* Cambridge University Press, New York.
Zwicknagl, G. and Fulde, P. (2003) *J. Phys.: Condens. Matter,* **15**, S1911.